Characterization studies of a GEM detector prototype for the ALICE TPC upgrade for LHC Run 3 and beyond

Olav Tegle Sande

University of Bergen
Department of Physics and Technology

Master Thesis

Supervisors:
Ph.D. Ganesh Tambave
Professor Dieter Rohrich

November 2016

Abstract

The multiwire proportional chamber signal readout of the ALICE Time Projection Chamber (TPC) will be replaced by Gas Electron Multiplier (GEM) detectors to meet the new requirements due to higher collision rate and energies during LHC Run 3 in 2018 and beyond. The GEM detector used in the ALICE TPC will vary from standard GEM detectors because it is designed to have a low ion back flow in order to have minimal distortion of the electric field in the TPC.

The focus of this thesis has been to characterize a GEM detector prototype using different types of radioactive sources. A goal has also been to make at setup for discharge studies with the GEM detector using both an external alpha source and an internal gaseous source.

The gain of the GEM detector prototype was calibrated at different operating voltages, detector gases and gas flow rates using a 5.9 keV photon source. The same source was used to measure the relative resolution. It was measured to be around 12 % at nominal gain of 2000. This is low compared to standard GEM detectors which might have resolution around 8 % at a 5.9 keV photon peak. This is due to the special specifications of the GEM detector prototype which aims to reduce the ion back flow.

The detector was also tested with minimum ionizing particles (MIPs) using a beta source. A setup with a plastic scintillator as an external trigger was used to discriminate the low energy electrons emitted from the beta source. The system had high noise when reading out the largest readout pad due to high input capacitance of the large readout area. It did not perform well and the gain had to be above the nominal gain of 2000 to get a clear Landau distribution from the MIPs.

An external alpha source was used to induce discharges in the detector. No discharge was observed at nominal gain but increasing the gain by a factor of about five made discharges happen. This setup only gives discharges in a small area where the source is pointing. A setup for discharge studies with gaseous alpha sources was made. Radioactive radon gas from a rock and thorium enriched mantles was added to the detector gas flow and used as sources. Using radioactive gas makes particles decay in the whole gaseous volume of the detector. The rate of alpha decays from these source was measured up to about 8 Hz with a $27 \times 27 mm^2$ readout pad.

After a lot of testing with different radioactive sources the relative energy resolution of 5.9 keV photons was measured again. The resolution for a detector setting was 15 % before all the testing but had decreased to 20 % afterwards. The detector may have been damaged by the alpha particles from the radon sources.

Acknowledgements

I would first like to thank you my supervisors Professor Dieter Rohrich and Ph. D. Ganesh Tambave. A special thanks to Ganesh for patiently helping and guiding me in through the daily work.

I would like thank all my friends and especially my class mates. You have made my time as a student memorable.

Furthermore, I would like to thank my family for the love and support throughout my life.

And lastly, special thanks to Keth and Eleah. Thank you Keth for being such a good wife and for being an excellent mother to Eleah. Thank you Eleah for being the the best daughter I could imagine. Thank you for all the smiles and fun we have together. I love you.

Bergen, November 2016

Olav Tegle Sande

Contents

Chapter 1

Introduction

Subatomic physics is the part of physics where the fundamental particles and their interactions are studied. Accelerators are used in modern subatomic physics to collied particles at high energies and study the outcome of these collisions in order to get information of how the particles interact. The conditions created in heavy ion collisions are thought to be similar to those of the earliest moments of the universe. Various types of particle detectors are needed to detect what is produced in these collisions in order to reconstruct what happen when the particles collide.

1.1 Large Hadron Collider (LHC)

The Large Hadron Collider (LHC) is the largest and most powerful particle accelerator ever built. It is designed to collide proton beams with a center-of-mass energies of up to 14 TeV for protons and Pb-ions with an energy of 5.5 TeV per nucleon [1]. It is built by CERN, the European Organization for Nuclear Research, and began to operate in 2008.

The machine is located in a 26.7 km long circular tunnel outside of Geneva, Switzerland. The particles are accelerated in two parallel beam lines in opposite directions. They can be collied at four points along the beam line. The four different experiments, ALICE, ATLAS, CMS and LHCb, are located at these points as shown in figure 1.1. The particles are accelerated in bunches with electric fields and steered in a circular path with superconducting magnets. The LHC is the last part of a large accelerator complex at CERN. The accelerator complex consisting of several smaller accelerator which accelerates protons to an energy of 450 GeV before they are injected into the LHC and accelerated up to the maximum energy of 8 TeV.

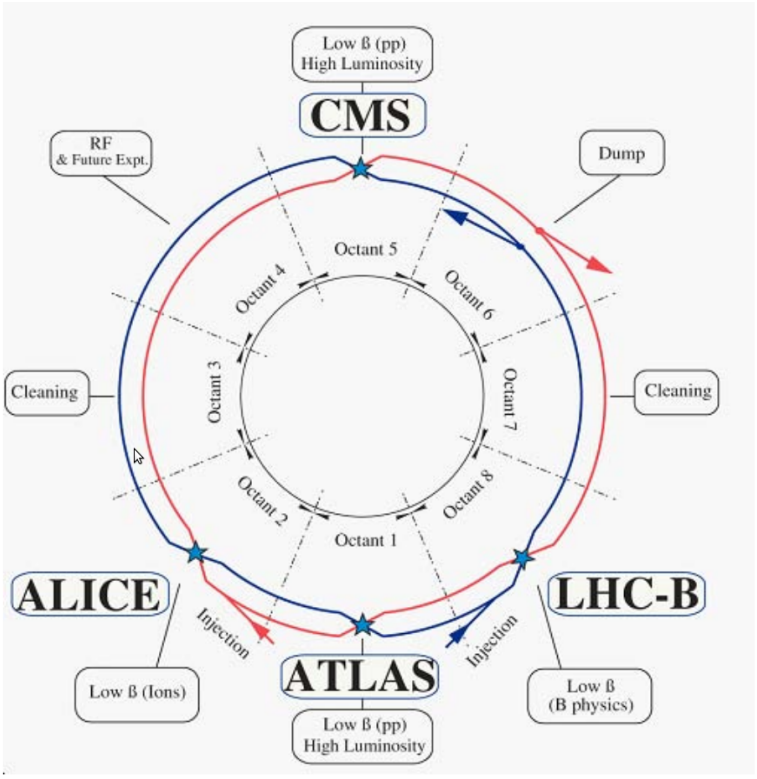

Figure 1.1: Schematic overview of the LHC and the experiments along the beam line [1].

1.2 The ALICE experiment

A Large Ion Collider Experiment (ALICE) is a general-purpose detector at the LHC at CERN. It aims to study the strongly interacting matter at extreme energy densities. This is done by colliding particles (protons and lead nucleons) with the high energies achieved by the LHC. At these energies head on collisions of lead ions create a quark-gluon plasma which is thought to be a condition similar to the state of the early universe about 10^{-4} s after the Big Bang. The temperature at this state is in about 10^{12} K. At this temperature the quarks and gluons are no longer confined inside hadrons but are free particles. It is then possible to study what happens when the quark-gluon plasma cools and forms ordinary matter. Some of the goals are to explain the properties of quark gluon plasm, why the quarks are confined inside of hadrons and why hadrons have much larger mass than the quarks they are made of.

The ALICE experiment consists of 18 different detector systems sketched in figure 1.2. It is designed on basis of what physics is going to be studied and the experimental conditions at the LHC. The most important parts are

the inner tracking system (ITS), the Time-Projection chamber (TPC), the Transition Radiation Detector (TRD), the Time-of-Flight detector (TOF), Ring Imaging Cherenkov Detector (HMPID), the electromagnetic calorimeters and the muon spectrometers. The ITS is the closest detector to the collision point and consists of six layers of silicon detectors and is used to detect short-lived particles. The TPC surrounds the ITS and is the main tracking device. It is a 90 m^2 gas filled cylindrical detector divided in two by a central high voltage electrode. Charged particles will ionize the gas when traversing through it. The electrons will then drift to the end caps where they are detected and they will give a two dimensional projection of the trajectory. A constant drift time gives the third coordinate to the trajectory and a three dimensional trajectory of the particles are recorded in the TPC. The electrons from the ionization process are currently read out at the end caps by MultiWire Proportional Chamber (MWPC) but will be replaced by GEM detectors after the current running period of the LHC. The TPC, TRD, TOF and HMPID are used for particle identification. The electromagnetic calorimeters are used to measure photons and the muon spectrometers are used to measure muons that are passing through the absorbers. The whole central part of the detector is placed in a solenoidal magnetic field which bends the trajectory of charged particles in order to measure their momentum [2].

1.3 LHC and ALICE upgrade

The LHC had its first long shutdown from 2013 to 2015 for maintenance and consolidation. The LHC is now running and will have a second long shutdown in 2018 where the LHC will be upgraded before Run 3. The interaction rate in Run 3 for Pb-Pb-collisions is expected to be 50 kHz. Several of the detector systems of ALICE will be upgrade to handle the increased interaction rate and to improve performance. The Time-Projection Chamber (TPC) of ALICE is one of the detectors that need to be upgraded in order to handle the increased interaction rate.

The currently used MultiWire Proportional Chambers (MWPC) for signal readout of the TPC is running at triggered readout with use of an active gating grid to block positive ions from drifting back into the TPC. The maximum TPC drift time is about 100 μs and the gating grid need to be closed for about 180 μs. This means that operation of the TPC at a collision rate of 50 kHz and average time between collision of 20 μs is not possible with active gating. The MWPCs will be replaced by Gas Electron Multiplier (GEM) detectors. The GEM detectors allow continuous readout and little ion back flow since most of the positive ions will be collected at the electrodes of the GEM detector. Along with the replacement of the readout detectors the front end electronics also need to be upgraded [3]. The GEM

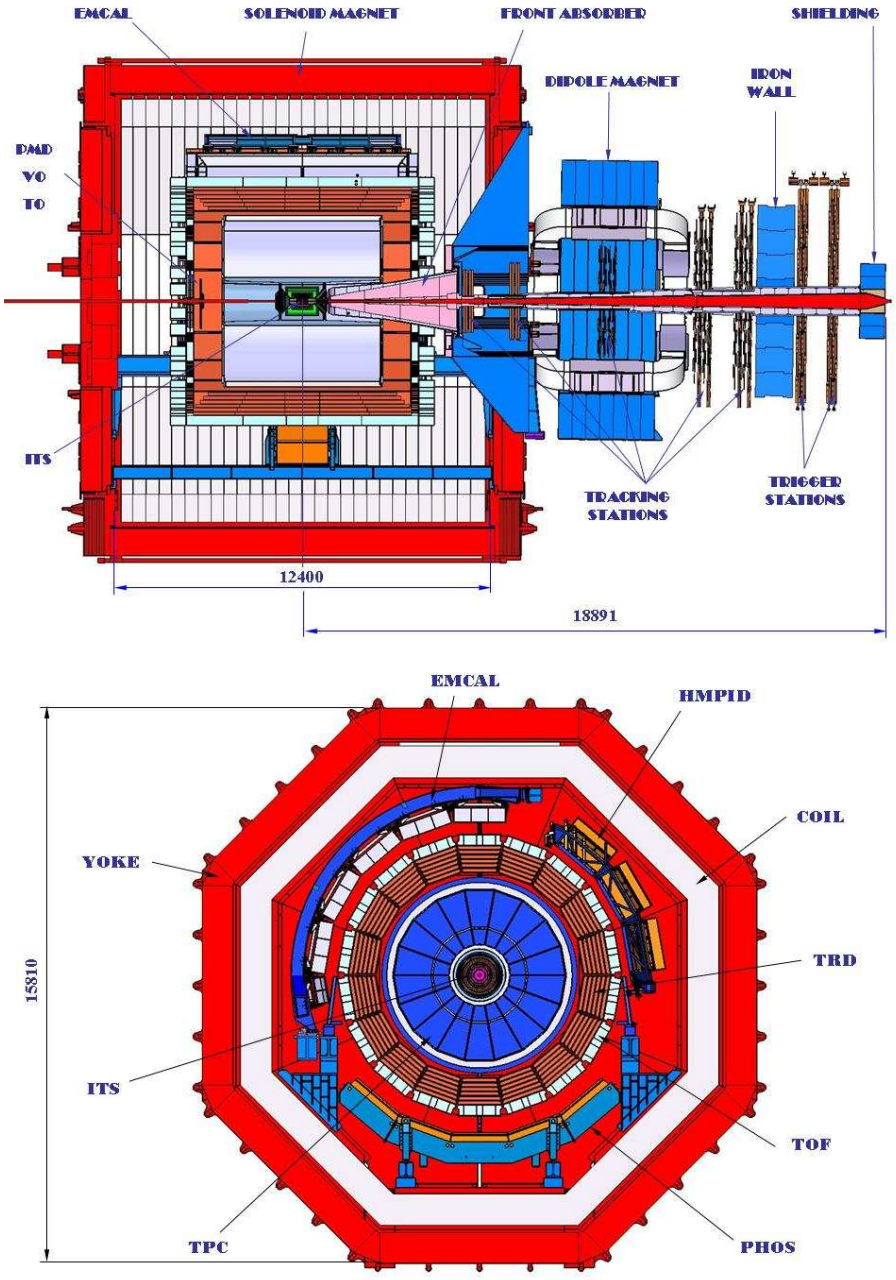

Figure 1.2: Two dimensional sketches the ALICE detector [2].

detectors will be read out using a readout chip called SAMPA. SAMPA is a custom made front end ASIC (Application-Specific Integrated Circuit) for several different subsystems of the ALICE detector.

1.4 Outline of the thesis

The goal of my master thesis work is first to test a GEM detector prototype together with the SAMPA readout chip which is specially designed for the ALICE TPC and the muon system. The detector prototype is tested with different types of radioactive sources and the radiation will be compared to each other.

The second part of the project was to make a setup for discharge testing of a the detector prototype with a radioactive gas and characterize this source.

The thesis is divided into seven chapters, including the current introduction chapter. Chapter 2 provides a short overview of how particles interact with matter which is the foundation of how signals are formed in a gas detector. Chapter 3 describes how GEM detectors work and how the GEM detector prototype is constructed. Chapter 4 shows the results of the gain calibration and measurements of the relative energy resolution. Chapter 5 contains the results of measurements with minimum ionizing particles. Chapter 6 is about measurements with different alpha source and how this is related to discharge studies with a GEM detector. At last chapter 7 summarize and concludes the thesis

Chapter 2

Interaction of particles with matter

In order to get a signal from a particle, it need to interact with the detector in a sensitive volume and lose some energy there. Particles lose their energy in different ways in matter depending on the particle type, energy and the properties of the matter. Different types of particles will therefore interact and lose energy in different ways in the sensitive volume of a gaseous detector. It is convenient to distinguish between charged particles and photons. Example of charge particles are the charged leptons (electrons and muons) and charged hadrons like protons, heavier ions and charged pions. Neutral particles like neutron and neutral pions are not ionizing and will not leave signals directly in the detector but secondary particles from (nuclear)reaction do. This is not relevant for most gas detectors.

2.1 Energy loss of charged particles

To describe the energy loss of charged particles we have to distinguish between the so called heavy charged particles and electrons/positrons.

Heavy charged particles have a much larger mass than the electron, $m_0 >> m_e$. They lose their energy mainly through inelastic collisions with atomic electrons of the traversed media. The atoms will be both exited and ionized. Charge particles can also be deflected from the incident direction through elastic scattering from the atomic nuclei of the matter. The energy loss from collisions with atomic electrons is approximately described by the Bethe-Bloch equation which gives the average energy loss per unit length $\frac{dE}{dx}$. The energy loss can be expressed as[4]

$$-\frac{dE}{dx} = K\varrho z^2 \frac{Z}{A}\frac{1}{\beta^2}[\frac{1}{2}ln(\frac{2m_e c^2\gamma^2\beta^2 Wmax}{I^2}) - \beta^2 - \frac{\delta}{2} - \frac{C}{Z}]$$

where $K = 4\pi N_A r_e^2 m_e c^2$ and W_{max} is the maximum energy transfer to a free electron in a single collision and is given by [4]

$$W_{max} = \frac{2m_e c^2 \beta^2 \gamma^2}{1 + 2\frac{m_e}{m}\sqrt{1+\beta^2\gamma^2} + (\frac{m_e}{m})^2}$$

Table 2.1 provides an overview of the variables used in the equation.

Symbol	Definition	Value and/or unit
r_e	Classical electron radius	2.818 fm
m_e	Electron mass	0.511 $MeVc^{-2}$
m	Mass of incident particle	$MeVc^{-2}$
ϱ	Density of absorbing material	gcm^{-3}
z	Charge of the incident particle	
Z	Atomic number of the material	
A	Atomic mass of the material	
β	$\frac{v}{c}$ of the incident particle	
γ	The Lorentz factor $\frac{1}{\sqrt{1-\beta^2}}$	
v	Speed of incident particle	ms^{-1}
c	Speed of light in vacuum	$2.998 \times 10^8 ms^{-1}$
W_{max}	Maximum energy transfer in a collision	
I	Mean excitation potential	eV
δ	Density correction	
C	Shell correction	

Table 2.1: The details of the variables used in the Bethe-Bloch equation.

Figure 2.1 shows the overall graph of the energy loss. The particles move slow at lower energy and have more time to interact with the matter and will therefore lose more energy per unit length. The rise at higher energies, called the logarithmic rise because of the logarithmic term, is mostly due to large energy transfers to a few electrons in the medium is possible at these energies because of flattened electric field in the traversed direction. The rise is reduced because of relativistic effects.

The Bethe-Bloch equation needs to be modified to apply for electrons and positrons. Much larger energy transfer is possible in one collision when the mass of the incident particle is the same as the electron of the traversed media. Electrons are in addition indistinguishable particles and need special treatment. Energy loss due to bremsstrahlung will in addition to ionization and excitation be more dominant for electrons and positron at relatively low energies because of the small mass.

The energy loss of charge particles is a statistical process. Charged particles will interact many times when traversing a layer of some material. If it is a thin layer and the number of interactions is low the energy loss

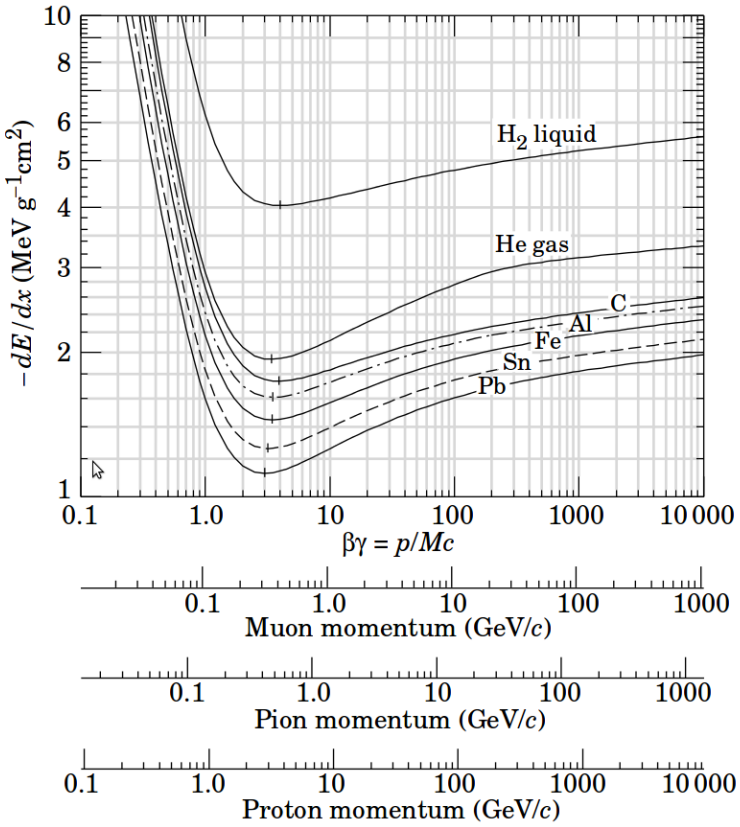

Figure 2.1: Energy loss of charged particles in different absorbers [5].

distribution will be Landau distributed. This distribution is asymmetrical due to possibilities for large energy transfers. The upper limit of the tail is the maximum energy transfer W_{max}. The mean of this distribution is larger than the most probable value. In a thick absorber such that the number of collisions is large the energy loss will be Gaussian [4].

2.1.1 Bremsstrahlung

At high energies charged particles also loose some of their energy by emitting photons when interacting with the atomic Coulomb field of the traversed medium. This is called bremsstrahlung. This is most relevant for electrons and positrons due to their low mass. The effect dominates at relativistic energies (> about 10 MeV) and is not an important effect for the beta source used for the tests with the GEM detector prototype.

Charge particles can also lose energy through mechanism like Cherenkov radiation, transition radiations and strong interactions of hadrons but this is not relevant for the test performed for this thesis.

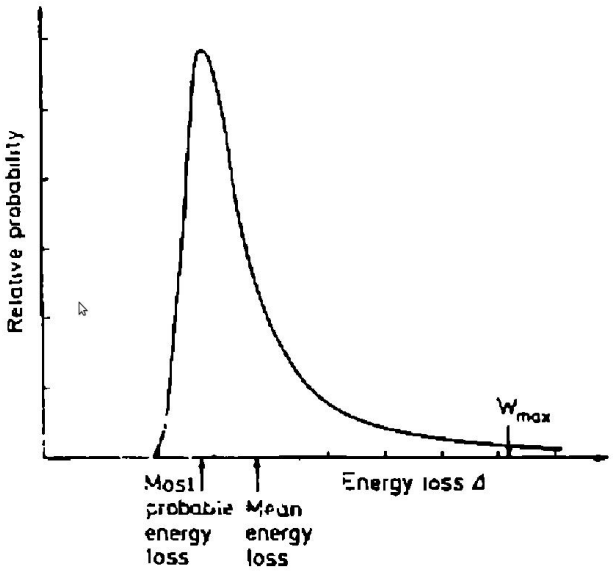

Figure 2.2: Energy loss distribution in a thin absorber. The tail at large energy is because of the possibility of large energy transfer in a single collision [4].

2.2 Energy loss of photons

Interaction of photons with matter are fundamentally different than for charged particles. Photons do not lose energy through many interactions, but are either absorbed or scattered through a relatively large angle in one interaction. The intensity of a photon beam is therefore reduced when a beam is going through matter. The attenuation is exponential and described by[6]

$$I = I_0 e^{-\mu x}$$

Photons are detected indirectly through the electrons produced when photons are interacting with matter.

2.2.1 Photoelectric effect

Photoelectric effect is when a photon is completely absorbed by an atomic electron. This is not possible for free electron since a third collision partner is needed in order to have momentum conservation. It is most probable to happen with the inner K-shell electrons since they are close to the nucleus which act as the third collision partner. It is the ionization from the outgoing electron that is measured in a gas detector. The energy of this electron is $E_e = E_\gamma - E_{binding}$. This effect is the most dominant effect at lower energies

($ionizationenergy \leq E_\gamma \leq 100keV$) but this varies a bit since the cross section is dependent of the atomic number Z [5].

The photoelectric effect was the most important interaction when the GEM detector prototype was tested using a Fe-55 radioactive source which emitted photons with an energy of 5.9 keV.

2.2.2 Compton effect

Compton effect is the process when a photon scatters off a quasi-free electron of an atom as shown in figure 2.3. The electron is treated as free and the binding energy is neglected. It is the ionization from the outgoing electron that is measured in a gas detector. The energy of this electron is

$$E_{\gamma'} = \frac{E_\gamma}{1 + \frac{E_\gamma}{m_e c^2}(1 - cos(\theta))}$$

The Compton effect have the largest cross section when the energy is about 1 MeV.

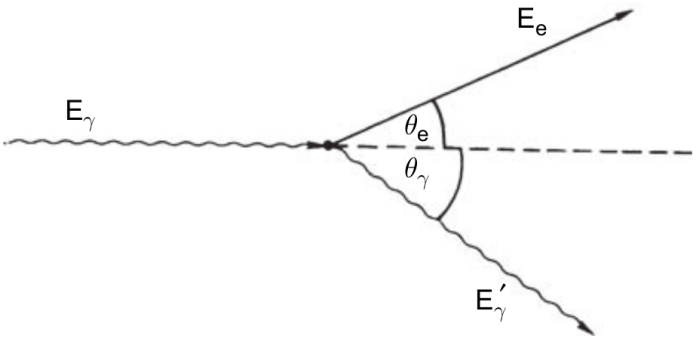

Figure 2.3: Schematic of variables of Compton scattering [6].

2.2.3 Pair production

Pair production happens when a photon interacts with the Coulomb field of a nucleus (or electron) and produces an electron-positron pair. This effect is most dominant at high energies ($\gg 1MeV$).

2.3 Electron avalanche

Electron avalanche is the process where a free electron is accelerated by a strong electric field and gain enough energy to ionize a new atom and create

new free electrons. The newly freed electron will also be accelerated by the electric field and cause further ionizations. This will create an avalanche of electrons. Many gaseous detectors have a region with a strong electric field where electrons from the primary ionization process drifts into and then forming an electron avalanche which is then read out from the detector. The detectors will then give a larger signal and have larger signal to noise ratio.

Electrons have higher mobility than ions and will drift faster in an electric field. This results in a liquid drop shape of the electron avalanche. The electrons will be grouped together with while the slow ions will form a tail [6].

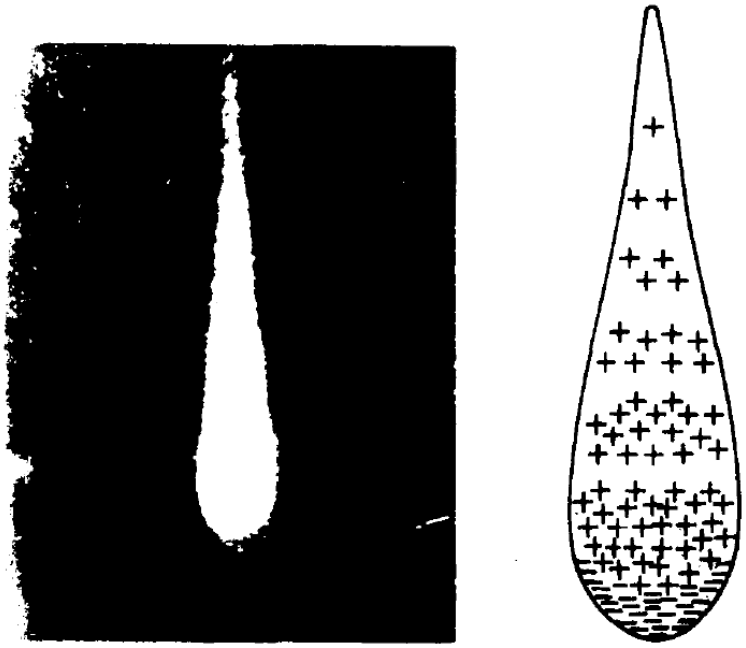

Figure 2.4: The left figure is a picture of an electron avalanche from a cloud chamber[6]. The right figure is an illustration of how the electrons and the ions are distributed in an avalanche [4].

Chapter 3

GEM Detector Prototype

A Gas Electron Multiplier (GEM) detector is a gaseous detector originally developed for particle physics by F. Sauli in 1997 [7]. Today it has large number of application. The GEM detector will be used as readout detector from the ALICE Time Projection Chamber for Run 3 in 2018 and beyond.

3.1 Gas Detectors

There are a large number of different gas detectors. The basic principle is that the detector has a gas filled volume and two or more electrodes which makes an electric field in the gas. When ionizing particles are traversing through the gas-filled volume they will ionize the gas. Because of the electric field the electrons and the positive ions will drift in the gas in opposite direction. Both the electrons and the ions can be collected on the electrodes giving an electric signal. In many cases the gas detectors need to have some kind of amplification of the electrons or ions in order to have a large enough signal to read out. The common way to do this is to make a region where the electric field is very strong. If the electrons from the primary ionization process drifts into a large enough electric field they will be accelerated and ionize the gas giving rise to an electron avalanche. The electrons will be collected on one of the electrodes. The electrons or the mirror charge of will produce an electric signal. Detectors with this kind of amplification are called proportional counters [6]. The Geigen-Müller counter and the Gas Electron Multiplier (GEM) detector are example of gaseous detectors.

3.2 GEM detector constituents

A typical Gas Electron Multiplier (GEM) detector is sketched in figure 3.1. The most important parts are the cathode, anode, GEM foils and the space between them. These parts are placed in an air tight chamber filled with an appropriate gas when operated.

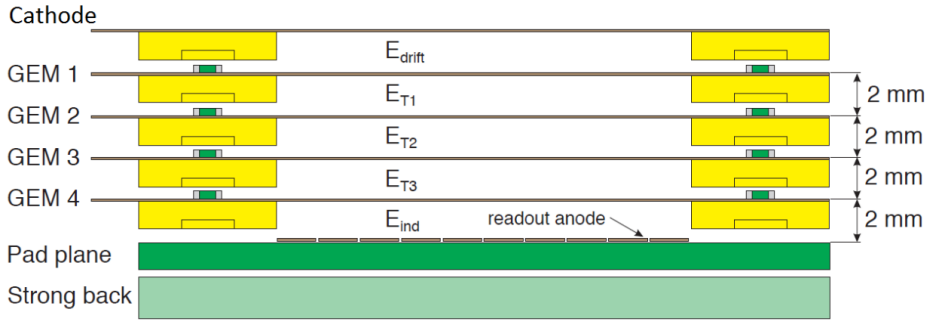

Figure 3.1: Constituents of a typical GEM detector with four GEM foils [3].

The cathode is connected to a high voltage supply and makes up the electric fields that make the electrons drift to the anode. It can be made of metal films, wires or wire-mesh.

The GEM foils are made of a polymer foil coated with metal on both side. The foil have a high density of holes and a potential difference between the metal coating on both sides making a large electric field in the holes. This is where the amplification happens. A photograph a GEM foil is viewed in figure 3.2.

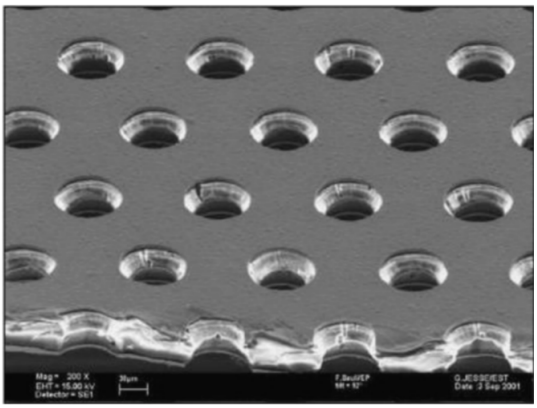

Figure 3.2: A picture taken by an electron microscope of a typical GEM foil. It is 50 μm thick, the hole pitch is 140 μm and the diameter of each hole is 70 μm [7].

The anode is where the signal is read out. This can be done several ways. The anode can consist of two dimensional strips or a segmented plane where each segment is connected to the readout electronics

The space between the electrodes are filled with an appropriate detector gas and there are electric fields in these regions. The top region is the sensitive volume of the detector and is where the particles ionize the gas.

This region is called the drift region. The electrons are transported to the top GEM foil, called GEM 1, by the electric field E_{drift}. The regions between the foils are called transfer regions and are where the electrons are transferred from one GEM foil to another between between the amplification happening in the GEM foils. The electric fields are called E_{T1}, E_{T2} and E_{T3} for a detector with four foils. The last region is the induction region with the electric field E_{ind}. This is where the electrons are transported to the read out anode. The electric fields and the foils are showed in figure 3.1.

3.3 GEM detector operation

The basic operation of a single foil GEM detector is shown in figure 3.3. An ionizing particle is going through the sensitive volume of the detector making ion and electron pairs. The electron drifts into a hole in the GEM foil because of the electric field. When passing through the holes of the GEM foil the electrons are accelerated enough to ionize even more. This gives rise to an electron avalanche. The electrons can then be transported by the electric field to one or several more GEM foils for further amplification. At last the electrons are drifting to the anode by the induction field. The electron avalanche is collected on pads or strips at the anode. The pads or strips are connected to the read out electronics.

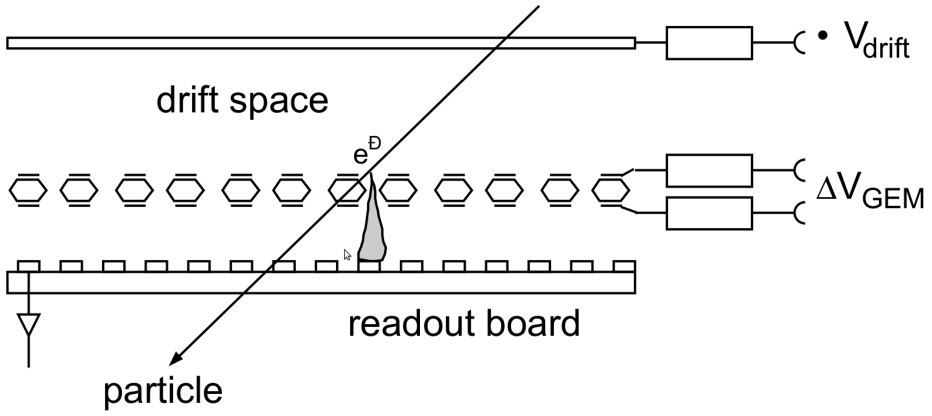

Figure 3.3: Basic operation of a GEM detector with only one GEM foil [6].

3.3.1 Gain

The gain is an important parameter of a GEM detector. The gain of a GEM foil describes the ratio of how many electrons leaving a hole to the number of electrons entering the hole. It is also convenient to talk about the effective gain of a detector. The effective gain is the ratio between the number of

electrons collected at the anode plane to the number of electrons from the primary ionization process in the gas from the particle being detected.

The gain of a GEM detector can easily be in the order of 10^5 for a multi foil GEM detector or 10^4 for single foil GEM detector. When heavily ionizing particles are present the maximum gain that the detector can safely be operated at is strongly reduced because of discharges. GEM detectors with several foils are generally safer to operate than a detector with only one foil at a given gain [8]. In a single GEM detector a high potential difference between the two sides of the GEM foil is needed to achieve gains of about thousands. Putting several GEM foils in one detector reduces the voltage needed at each GEM foil to achieve gains of thousands or even more.

The gain of the GEM detectors used for readout of the ALICE TPC will be 2000. This value is chosen since it ensure as high gain as possible to achieve a high signal to noise ratio and a small discharge probability. Figure 3.4 shows a measurement of the discharge probability and the gain in a GEM detector. The discharge probability is increasing a lot when the gain is large than some thousands [9].

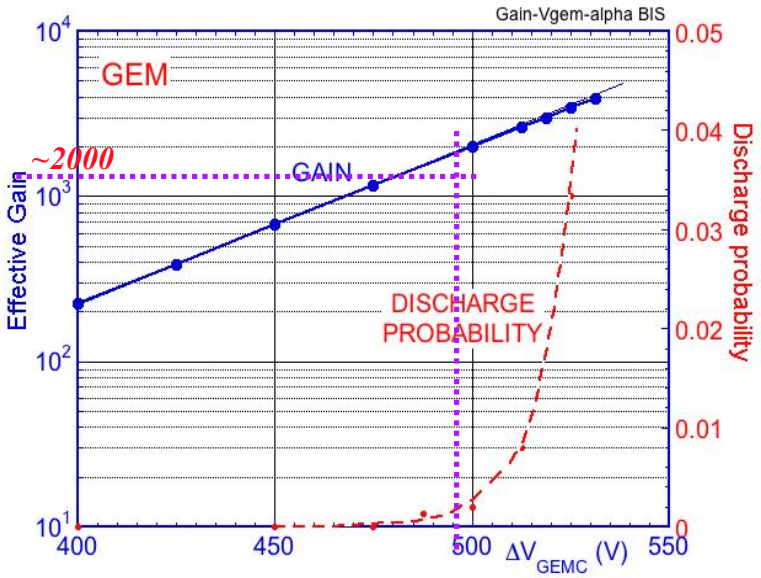

Figure 3.4: The gain and discharge probability plotted as a function of the GEM voltage measured with an alpha source [9].

3.3.2 Discharges

Discharges (sparks) are a limiting factor when operating a GEM detector and other types of micro-pattern gas detectors. Discharges occurs if there are a large amount of charges in the gas making a breakdown of the gas

and leading to a conducting bridge between electrodes in the detector. Discharges occur if the total number of electron-ion pairs exceed the Raether limit of about 10^7 [7]. Heavily ionizing particles creates many free charges in the detector and are therefore most likely to induce discharges. Discharges can be harmful for a detector especially if there is a conducting bridge to the readout electrode. If the large amount of charge is conducted to the front-end readout electronics it can destroy the electronics.

Protection circuits can be made by using resistors and diodes to reduce the amount of charge conducted to parts of the detector that can be easily damaged. Figure 3.5 shows an example of protection circuit in front of the front end electronics.

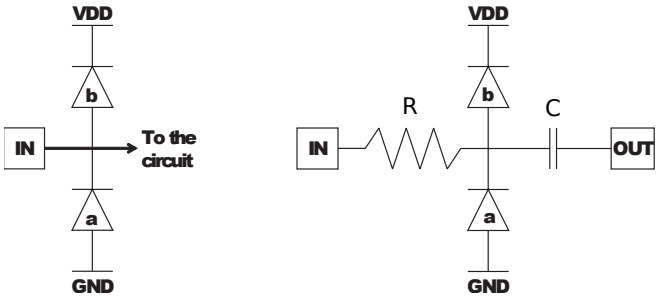

Figure 3.5: Standard discharge protection circuit to the left and improved protection circuit to the right [10]

The discharge probability is an important quantity and is defined as the ratio between the observed frequency of discharges and the source rate[8].

Discharge studies and testing of the protection circuit are performed by making discharges in a detector. To do this a radioactive source is usually used. Alpha source are used since alpha particles are heavily ionizing. Other types of sources can in principle also be used but the detector need to operate at a very high gain which may not be safe. The source can be placed either inside or outside the detector. If an external alpha source is going to be used the detector needs to have a thin window where the alpha particles can enter the sensitive gas filled volume and ionize. The alpha source can also be place inside the detector. This is often inconvenient since many detectors are designed operate in a pure gas mixture and it is not possible to open the detector to remove the source. This has to be done in a special clean-room. The advantages of this kinds of experiments are the high activity of the sources which will give high spark rates. One disadvantage is that the source only do exposure to a small area consisting of a few pads. This is not similar to conditions of large experiments. The local exposure from this setup however gives a defined energy spectrum [8].

The last option is to add a radioactive gas to the detector gas flow. Radon-220 from the thorium decay chain is commonly used for such stud-

ies. This will make radon decaying randomly in the whole detector volume possibly creating a lot of ionization which may create discharges. The energy distribution measured is broad. The use of Rn-220 together with the detector gas gives conditions more similar to the conditions of actual experiments where GEM detectors are used compared to the use of solid radioactive sources discussed in the previous paragraph. The cons with radioactive gas added to the detector gas is the low rate of the source leading to a low rate of sparks and it is therefore difficult to measure low discharge possibilities [8].

Sparks will usually not occur at nominal voltages for a GEM detector with several foils. The gain of the detector need to be several thousand to have a good rate of discharges. Discharge studies can therefore not be done at nominal gains but must be performed at much higher gains. However discharges may happen at low gains if the detector has only one foil [8].

3.3.3 Detector gas

A gaseous detector can in principle be operate in all types of gases but some give much better working conditions for the detectors than others. For proportional counters like GEM detectors this mean that the detector can be operated at low voltage, achieve high gain, have good proportionality and have high rate capabilities. Mixtures with a large component of a noble gases are commonly used to give the best operating conditions for a GEM detector.

Noble gases are used because they require the lowest electric field to form an electron avalanche. In addition, noble gases do not react chemically and are therefore stable under operation. Together with the noble gas a second gas called a quencher is needed. Noble gases usually have high excitation energy. Excited gas molecules de-excite by emitting a photon. These photons are capable to do unwanted ionization giving rise to further avalanches. Gases that absorb these photons are therefore added and called quenchers.

The ALICE TPC will be operating with a mixture of $Ne - CO_2 - N_2$ (90-10-5). In this mixture Ne is the main noble gas while CO_2 and N_2 are quenchers [3].

The Neon mix is preferred over an Argon mix because of the about three times higher mobility of Ne^+ than Ar^+. Higher mobility means that there will be lower space charge distortions of the electric field in the TPC [3].

3.4 Time projection chamber (TPC)

The time projection chamber (TPC) is a tracking detector used in many colliding beam experiments. A TPC consists of a gas filled cylinder dived in two by a central electrode. Particles are collided into each other in the center of the cylinder so that particles from collision are flying out in all direction.

Charged particles will ionize the gas. The central electrode makes electric filed which will ensure that ionized electrons are drifting toward the end caps of the TPC. The electrons are amplified and read out at the end cap. Multi Wire Proportional Chambers (MWPC) are historically most used. The ALICE TPC has used MWPC so far but will use GEM detectors as read out technology after the next upgrade in 2018.

The TPC is three dimensional tracking device. The signals from the end caps will provide a two dimensional projection of the particle path. The last coordinate is obtained from the constant drift velocity of the electrons. The signal at the end cap will also give information of the energy loss, dE/dx of the particles and give particle identification in certain energy ranges. Another advantage of a TPC is that the particles traverse very little material which keeps the multiple scattering at a minimum.

A TPC is placed in an magnetic field which is parallel to the electric field. Charged particles will have a curved path and the momentum of the particles can be calculated from the curvature of the path. The magnetic field also reduces the diffusion of primary ionized electrons while they are drifting towards the end caps. The electrons will spiral around the magnetic field direction.

A problem for a TPC can be that the positive ions from the amplification process drift back into the sensitive volume. This will distort the electric field and therefore change the drift time of the electrons. This is especially a problem when MWPCs are used as readout technology. Some kind of gating is then needed. This means that the detector have dead time when the gate is closed and will therefore be a problem at high rate experiments. This is the reason why the MWPCs are replaced by GEM detectors as the read out technology at the ALICE TPC. The GEM detectors have little ion flow back since most of the ions are collected at the GEM electrodes. Optimization of the GEM voltages and the electric fields together with the distances between the center of the holes in the GEM foils will also ensure a low ion back flow in the ALICE TPC [3]. The use of gating is not needed anymore and this allows a continuous operation of the ALICE TPC.

3.5 The GEM detector prototype

The GEM detector prototype at the University of Bergen used for measurement in this thesis has four GEM foils, a wire mesh cathode plane and anode readout plane divided into several pads of different size. The GEM foils have both standard (S) and large (LP) pitch size. The standard and large pitch size means that the distance between the center of the holes are 140 μm and 280 μm, respectively. The configuration is S-LP-LP-S meaning it has standard pitch size on the top and on the bottom and two foils with large pitch size in the middle as shown in figure 3.7. This is found to be

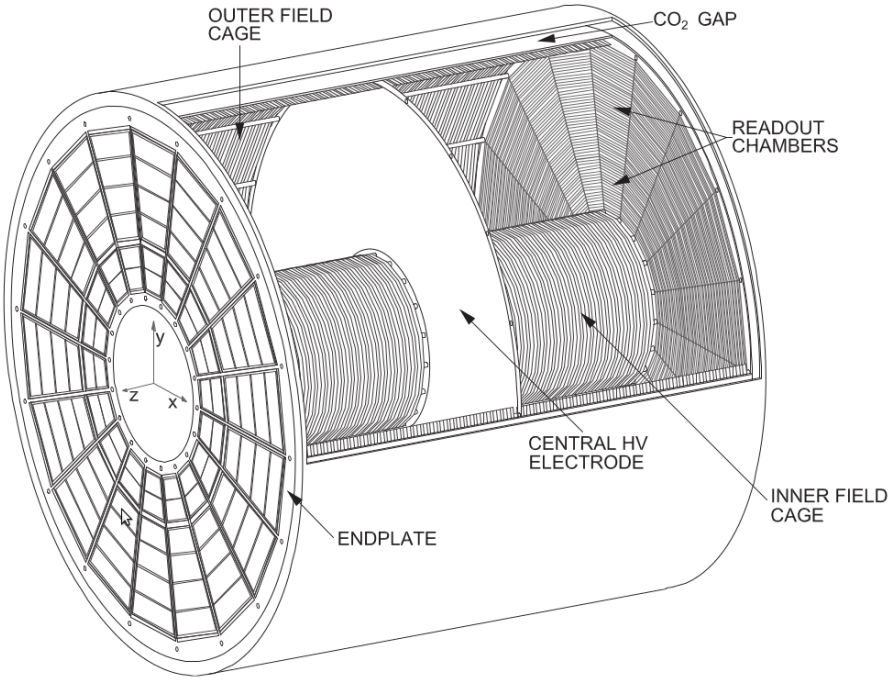

Figure 3.6: Schematic view of the current TPC in use at the ALICE experiment [3].

the best option for the ALICE TPC. Together with the optimal voltages this configuration has a low ion back flow ($< 1\%$) and acceptable energy resolution (about 12 %)[3].

3.5.1 Construction

The electrodes of the GEM detector is separated by special spacers seen in figure 3.8. The spacers make up the drift, transfer and induction regions. The drift region is only 5.6 mm in the GEM detector prototype. A larger region would be preferable since the incoming particles would have a large space to deposit their energy and therefore give larger signals. The size of the transfer regions is 2 mm while the size of the induction region is 2.3 mm.

The GEM foils are placed in a air tight container since the detector performs best in a pure gas mixture. The presence of electronegative gases like oxygen is specially unwanted. The container is made out of transparent plastic. The high voltage wires goes through the walls of the container and to high voltage supply and the resistor. The detector is sealed off at the top and the bottom with the cathode and the anode together o-rings to make it air-tight.

Figure 3.9 shows that the top cover above the cathode has five thin

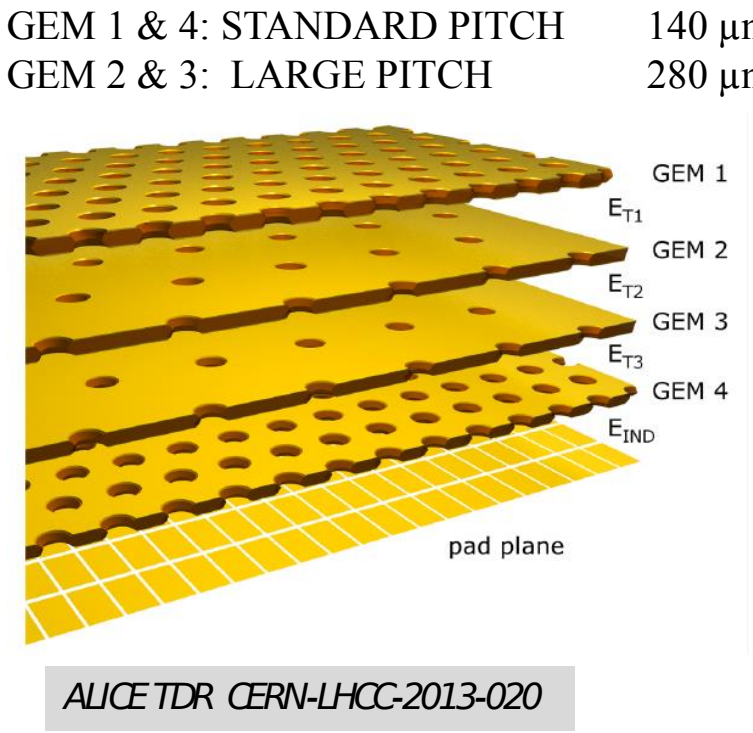

Figure 3.7: Schematic view of the GEM foil configuration of the ALICE TPC[3].

micron polymer windows to allow measurement with an alpha source outside of the detector. These windows are located over the pads to the left in figure 3.10.

3.5.2 Anode plane

The anode plane is made from a PCB (Printed Circuit Board). The PCB is rigid and the copper layer is segmented into pads and are used as the anode electrode. Each pad is connected to a pin on the other side of the PCB and this is where the signal from the detector is read out.

The anode plane of the detector has several different pads sizes and possibilities to read out different combinations of pads at the same time. A schematic view of the anode with different pads are showed in figure 3.10. At the bottom right corner is the large pad ($27 \times 27 mm^2$) used for gain calibration, measurements of the relative resolution and other types of testing. Pads with this size will not be a part of the ALICE TPC. The pads with sizes $6 \times 15 mm^2$ and $6 \times 10 mm^2$ have the same sizes as the pads that will be used for the outer and inner part of the outer readout chamber of the ALICE TPC. The smallest pads with size $4 \times 7.5 mm^2$ will be used for the inner read out chamber of the TPC.

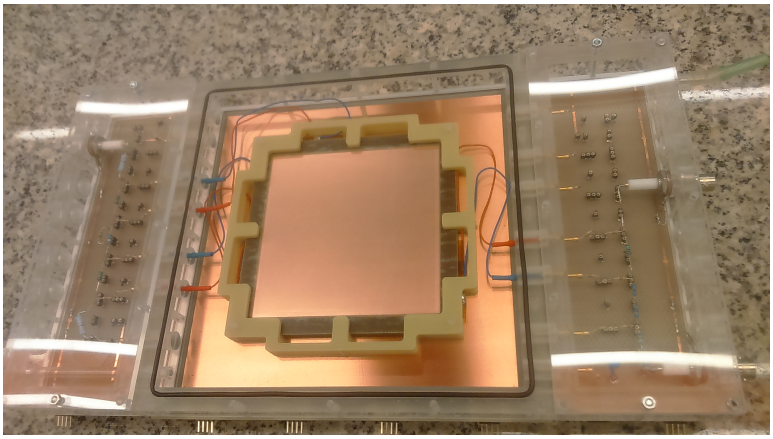

Figure 3.8: Photo of the detector before the cathode was mounted. The first GEM foil is shown with a spacer on the top. The size of each GEM foil is $10 \times 10 cm^2$. The blue and red wires connect the electrodes to the resistor chain. The resistors are visible to the left and right of the photograph. The frame on top and around the GEM foil is one of the spacers.

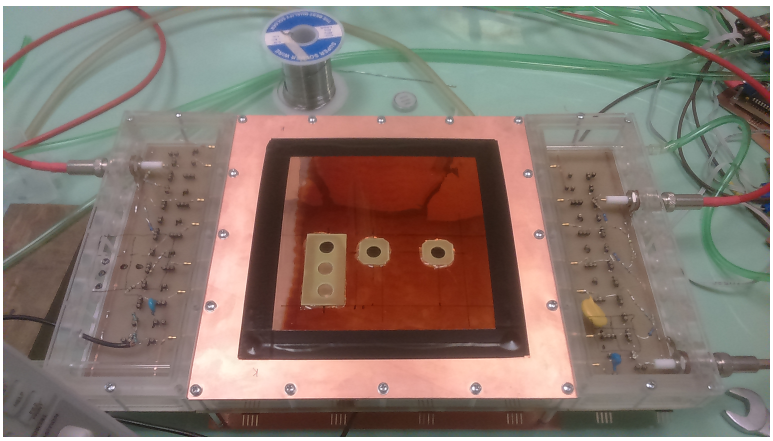

Figure 3.9: Photo of the detector with the cathode mounted. The five circular openings for passage of alpha particles are visible.

3.5.3 Resistor chain

The GEM detector prototype is powered by one high voltage power supply. The detector has a resistor chain which divides the high voltage so that each element in the detector is run by the correct voltage. This is done by resistor R3 to R11 as seen in figure 3.11. Resistor R2 and all the resistors named R in the same figure are protective resistors used to reduce the current in case of discharges. Resistor R1 and capacitor C creates a low pass filter reducing the noise from the power supply.

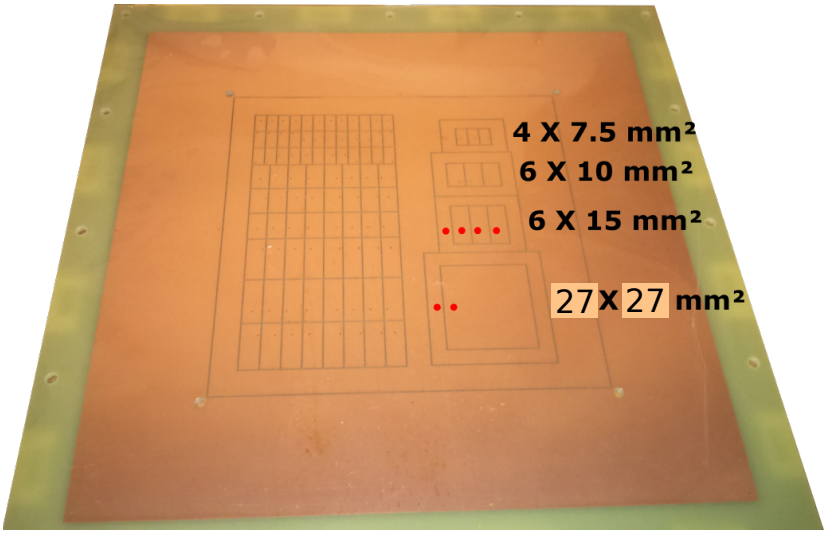

Figure 3.10: Schematic view of the anode pad plane of the GEM prototype. The small green dots are were the pads are connected to a readout pin.

Table 3.1 shows the voltages and electric field size the chamber need to run at 2000 gain in $Ne - CO_2 - N_2$ (90 % + 10 % + 5 %) gas mix. This corresponds to an operating voltage of 3.55 kV. Other voltages are required for achieving gain of 2000 in other gas mixtures. The detector requires higher voltage if operated in $Ar - CO_2$ (90 % + 10 %) gas since the number of primary charge created in the argon gas mix is higher. This will be further discussed in section 4.1.

Parameter	Voltage	Electric field
Drift field		400 V/cm
GEM1	275 V	
Transfer 1		4000 V/cm
GEM2	235 V	
Transfer 2		2000 V/cm
GEM3	284 V	
Transfer 3		100 V/cm
GEM4	345 V	
Transfer 4		4000 V/cm

Table 3.1: Table of voltages and electric field of of typical setting of the GEM prototype detector when operating in a $Ne - CO_2 - N_2$ (90-10-5) gas mix.

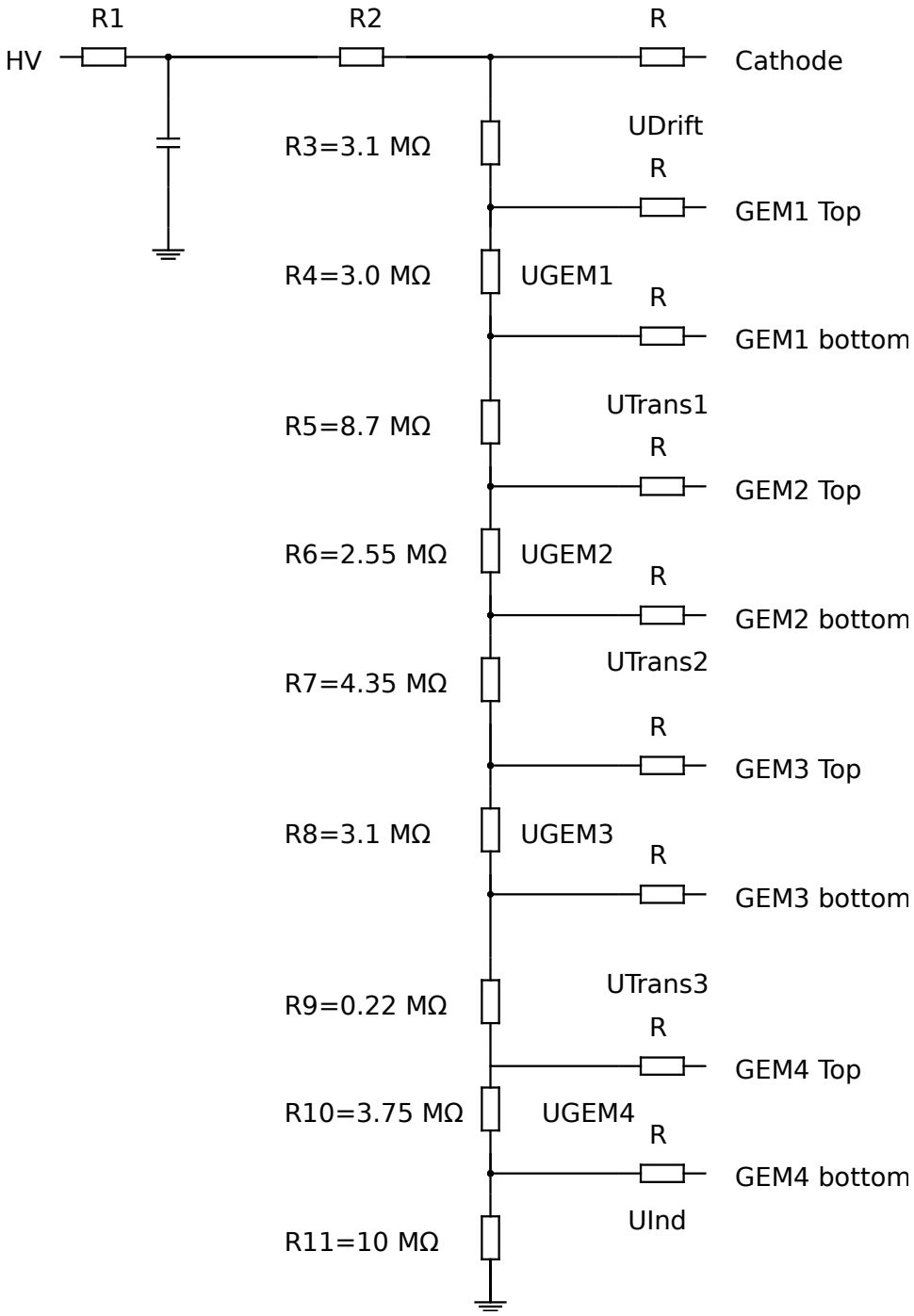

Figure 3.11: Schematic view of the resistor chain.

3.6 The SAMPA readout chip

The signals from the GEM detector prototype were read out using a SAMPA chip. The SAMPA chip is a custom made front end ASIC (Application-Specific Integrated Circuit) that will be used for both the ALICE muon tracking detector and the ALICE TPC readout. The SAMPA chip will replace the currently used readout chips of the ALICE TPC in order to match the new GEM readout technology and increased data rates. The inputs of the SAMPA chip are connected to the pads of the readout plane of the GEM detector.

Each SAMPA chip used in the ALICE TPC will have 32 channels but a prototype with only five channels was used for the measurements done for this thesis. This prototype was mounted on a carrier board and is shown in figure 3.12.

Each channel of the SAMPA chip consists of a Charge Sensitive Amplifier (CSA), a signal shaping circuit, an Analog-to-Digital Converter (ADC) and Digital Signal Processing (DSP) chain. The CSA first converts the current from the detector into differential semi Gaussian voltage signals. The shaping circuit tries to make constant peaking time and signal width. The signal is then digitized by the ADC. At the end the signals are processed and compressed by the DSP[3].

The SAMPA chip can be used at different settings since it will be used for both the muon chamber and the TPC. It has options which enables it to be used with both types of polarity, different sensitivities and different peaking times.

A typical differential signal output from the SAMPA chip is shown in figure 3.13. The peaking time is here about 160 ns which is the peaking time setting that will be used for the ALICE TPC. The peaking setting used for the muon chambers will be 300 ns.

During the measurements done for this thesis the signals were send from the SAMPA chip output to a CAEN ADC. The digital signals were then stored using LabVIEW[13]. The SAMPA chip is not designed for 50 Ω but the CAEN ADC used is 50 Ω terminated. A previous master student designed a buffer for impedance matching of the ADC and the SAMPA chip[12].

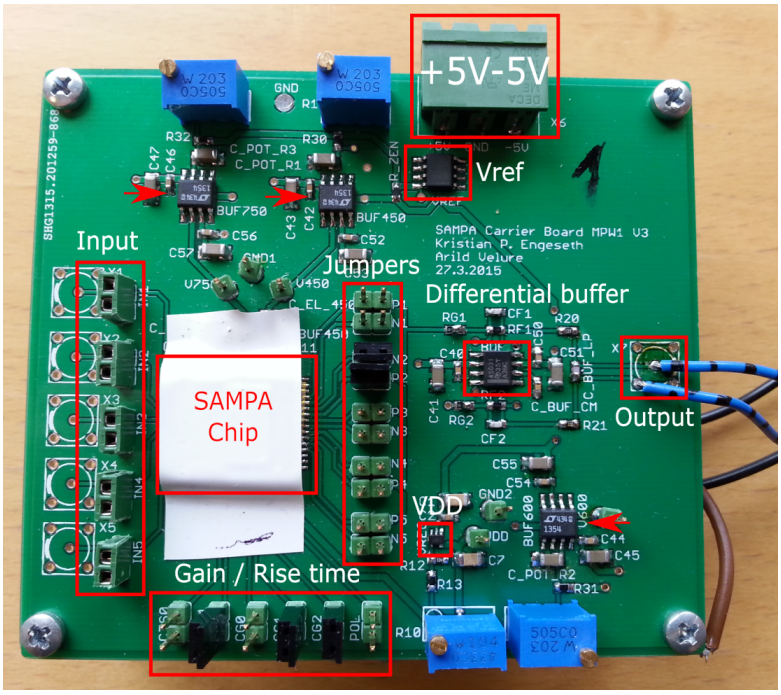

Figure 3.12: Picture of the SAMPA carrier board used for measurements in the thesis.

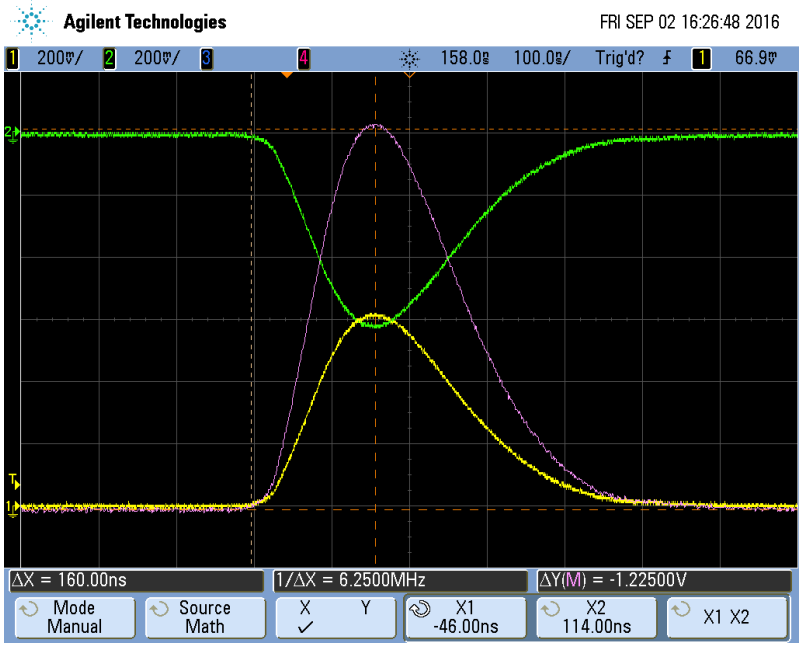

Figure 3.13: Picture taken by an oscilloscope of the differential signals from the SAMPA chip (yellow and green) and the difference between the positive and negative signal (pink).

Chapter 4

Gain calibration and energy resolution measurements of the GEM detector prototype

The GEM detector prototype was tested with a Fe-55 X-ray source for gain calibration and measurements of the energy resolution. Fe-55 decays by electron capture and is considered as a mono-energetic X-ray source with an energy of 5.9 keV. The activity was 37 MBq. This source was used to calibrate the gain of the detector and to obtain the the resolution at different detector settings.

The spectrum measured from the source in two different gas mixtures is shown in figure 4.1. These spectra are maximum amplitude histogram. The maximum values of signals are stored and filled into histograms. The main peak in both of the spectra occurs because of the photoelectric effect. The incoming photon hits in most cases an inner shell electron of the gas atoms in the sensitive volume, and kicks it out. This electron will do some further ionization. The electric field will make the electrons drift towards the GEM foils and be amplified. Finally the electrons will drift to the induction gap and they will be read out at the anode plane.

The spectrum obtained in the Argon gas mix has a second smaller peak. This peak comes from the filling of the inner shell vacancy. When an inner shell electron is kicked out an outer shell electron will fill the hole by emitting an photon to come in a lower energy state. In the case of argon the energy difference between outer and inner electrons is large enough so that the emitted photon can ionize the gas even more and will therefore create a second peak at lower energy. The number of counts of this peak is lower than for the main peak for several reasons. The incoming photons do not always interact with the inner shell electrons but can also interact with the outer electrons. Another reason is that the emitted photon from the filling of the inner shell is emitted in all directions and will not always do ionization

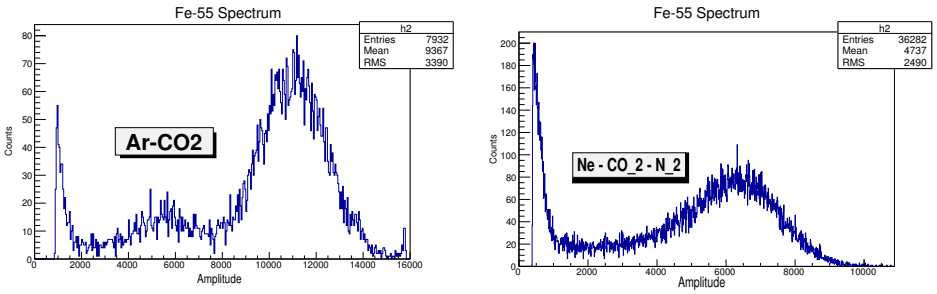

Figure 4.1: Fe55 energy spectra measured in $Ar - CO_2$ (90 % + 10 %) and $Ne - CO_2 - N_2$ (90 % + 10 % + 5 %) gas mixtures.

in the sensitive volume. Lastly the detector gas also consist of CO_2 which also will be ionized.

The leftmost peak at is due to noise from the detector, the SAMPA read-out chip and the data acquisition system. There are no counts at the lowest amplitudes. This is well within the range of the noise. When measuring the spectra a threshold was set above the noise.

4.1 Gain calibration

The effective gain of the detector was measured in two different gas mixes at different gas flow and GEM operating voltages. A goal was to find when the gain was about 2000 since the ALICE TPC will be operated at this gain.

The effective gain of the detector is defined as ratio between the number of electrons read out of the anode pads to the number of electrons from the primary ionization process in the gas in the drift volume. This can be expressed as

$$G_{eff} = \frac{I_{anode}}{e * N_{primary} * R}$$

were I_{anode} is the current read out on the pad, e is the elementary charge, $N_{primary}$ is the number of primary ionization and R is the rate of the incident particles.

The number of primary ionization in the gas mix from a 5.9 keV X-ray can be calculated from the value of average energy loss W, per produced electron-ion pair in the detector gas. The W values for some gases often used in gas detectors are shown in the table 4.1.

For the gas mix $Ar - CO_2$ (90-10), the ionization energy is

$$E_{ionization} = 0.9 * 26eV + 0.1 * 33eV = 26.7eV$$

Gas	Average ionization energy W [eV]
Ar	26
CO_2	33
Ne	36
N_2	35

Table 4.1: Average ionization energy in some commonly used detector gases.

The number of primary ionizations of a 5.9 keV X-ray is

$$N_{primary} = \frac{5.9keV}{26.7eV} = 221$$

For the gas mix $Ne - CO_2 - N_2$ (90-10-5) it is also needed to find the correct percentage of each gas since (90-10-5) means that 5 % of N_2 is added to a (90-10) mix of $Ne - CO_2$.

$$0.95 * 0.9 + 0.95 * 0.1 + 0.5 = 0.855 + 0.095 + 5 \rightarrow (85.5 - 9.5 - 5)$$

The ionization energy of the Ne-mix is

$$E_{ionization} = 0.855 * 36eV + 0.095 * 33eV + 0.05 * 35 = 35.67eV$$

The number of primary ionizations in the Ne-mix is

$$N_{primary} = \frac{5.9keV}{35.57eV} \approx 165$$

The gain of the detector is calculated using the Fe-55 source, the GEM detector, an oscilloscope and a microamperemeter. A picture of the setup is shown in figure 4.2. The measurements were done in both $Ar - CO_2$ (90-10) and $Ne - CO_2 - N_2$ (90-10-5) gas mixes at two different gas flow rates and at several different detector operating voltages. The source were placed on the top of the GEM detector pointing at the large pad ($27 \times 27mm^2$). The readout pin was connected to a microamperemeter which measured the current on the anode from the amplified signal from the detector. The readout pin was also connected to the SAMPA chip which send the signal to an oscilloscope to measure the rate of signals.

The gain measurement was tricky since the current was fluctuating and therefore not easy to determine. A way of improving this could be to measure the average current over some time using the microamperemeter and a computer with LabVIEW[13]. The rate from the source hitting the detector is constant at different operating voltage since the source is not changing. However the rate measured with an oscilloscope is not constant since the measured rate is inversely proportional to the trigger threshold of the oscilloscope. Higher voltages gave higher signal and it was possible to trigger at

lower signal values relative to the peak. This leave some room to measure different rates with the same source. The trigger threshold was kept slightly above the noise for all measurements.

The results of the measurements are displayed in figure 4.3. The gain seems to be linear in the operating voltage range.

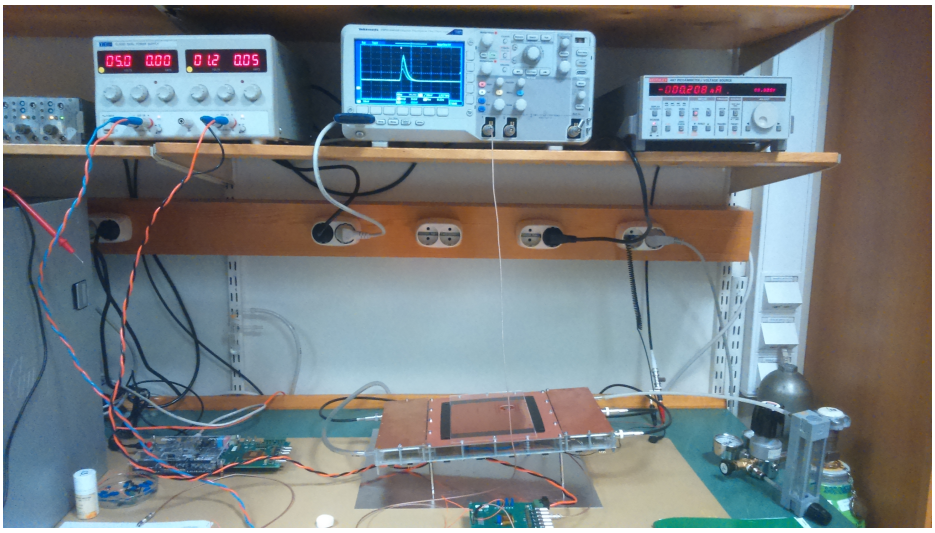

Figure 4.2: The set-up of the gain measurements. At the top from the left is the power supply, the oscilloscope and the microamperemeter. The GEM detector prototype and the gas system are at the bottom of the picture.

The gain of the detector in the $Ne - CO_2 - N_2$ gas mix is higher than in the $Ar - CO_2$ gas mix for the same voltage. This is due to the higher number of primary charge created in the argon gas mix compared to the neon gas mix.

It is clear from all of the measurements that a high gas flow through the detector gave higher gain. This is probably due to variation in the oxygen level in the detector. Some oxygen will leak into the detector but a higher gas flow rate will reduce the amount of oxygen in the sensitive volume of the detector. Oxygen(O_2) is electro-negative and electron will attach to the oxygen molecule. Some of the charge produced in the ionization processes will be lost. The gain of the detector will be reduced if oxygen are present.

This also shows the importance of the purity of the detector gas. The detector need to be placed in an air tight container and have a stable gas supply in order to achieve stable operation of the detector.

Gain of 2000 which the ALICE TPC will operate at is achieved with a operating voltage of about 3.55-3.6 kV in the $Ne-CO_2-N_2$ (90+10+5) gas mix depending on the gas flow rate. If the detector gas is the $Ar+CO_2$(90+10) gas mix the operating voltage need to be 3.75-3.8 kV depending on the gas flow rate.

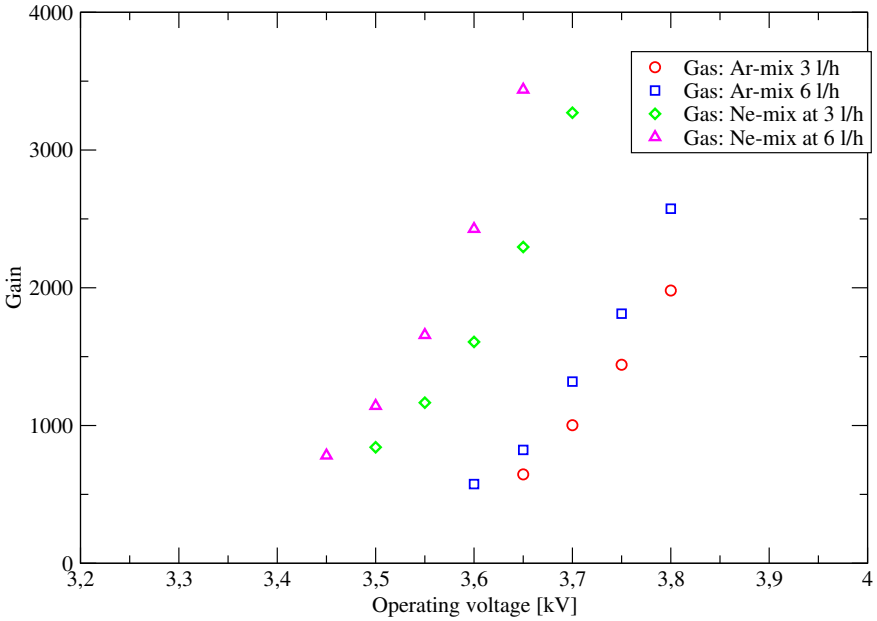

Figure 4.3: The gain of the chamber in $Ar{+}CO_2(90{+}10)$ and $Ne{+}CO_2{+}N_2$ (90+10+5) at different voltage and different gas flow rates in litres per hour. The gain was measured with the large pad ($27 \times 27mm^2$).

4.2 Resolution measurements

The energy resolution of a detector is an important quantity that tells how well the detector can measure the energy of a particle. The relative energy resolution is defined as the ratio between the standard deviation and the mean value of a energy distribution. For the ALICE TPC this is important for particle identifications at of certain particles at certain energy ranges.

The relative resolution of the detector from 5.9 keV photons was measured. The relative resolution was found by doing a Gaussian fit to the main peak in the Fe-55 spectrum. The standard deviation and mean were then found from the fit and used to calculate the relative resolution. The solid red line in figure 4.4 shows a fit to the spectrum from the Fe-55 source. The measurements where done at different operating voltages, two different gas flow rates and the signal was read out from different pad sizes.

The SAMPA chip was used to read out the signal. The chip gives out differential signals. The signal was acquired by a computer with LabView which saved the maximum amplitude of each signal. Figure 4.4 shows a spectrum from the Fe-55 source. The large right peak corresponds to the process where a 5.9 keV photon kicks out an inner shell electron. It is the ionization from this electron that is detected. The small peak just below channel number 4000 comes from filling of the inner shell vacancy. Signals

below about 2000 are noise.

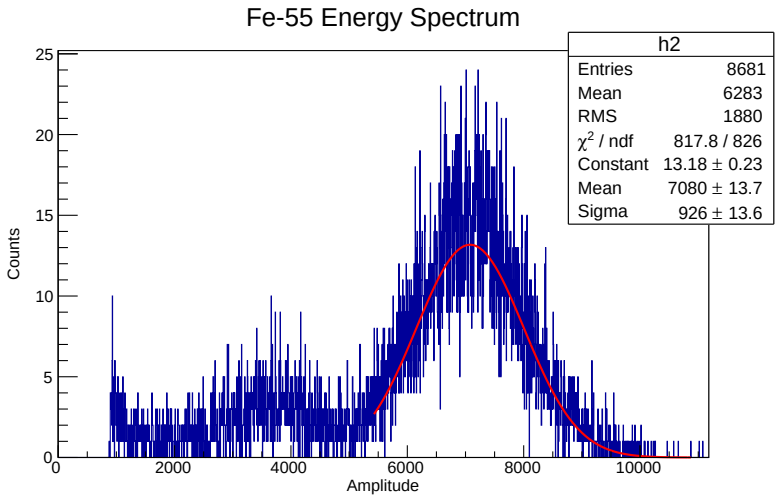

Figure 4.4: A Fe-55 spectrum measured in $Ar + CO_2(90 + 10)$ at a flow rate of 6 l/h. The operating voltage was 3.75 kV. The mean and sigma of the peak are 7080 and 926. This gives 926/7080 = 0.13079 which means that the relative energy resolution at 5.9 keV is about 13.1 %.

Measurements where done reading out different pads. The source was placed on the top of the detector pointing at the pads being read out in all of the measurements.

It is clear from all of the measurements that a high gas flow through the detector gave a better resolution. This is probably due to variation in the oxygen level in the detector. Electrons will attach to the electro-negative oxygen molecule. Some of the charge produced in the ionization processes will be lost. This will broaden the energy peak and make the the energy resolution lower. Some oxygen will leak into the detector but a higher gas flow rate will reduce the amount of oxygen in the detector volume.

Figure 4.5 shows the resolution measured with the large pad ($27 \times 27mm^2$). As we can see, the resolution is about 12 % at the best. The requirement for the energy resolution at 5.9 keV photon peak is 12 % for the GEM readout at the ALICE TPC.

Measurements reading out three normal pads ($6 \times 15mm^2$) at the same time were also done. As figure 4.6 shows, this gave as expected a lower resolution compared to measurements done on the large pad. The lower resolution is due to a smaller area being read out. This means that not all of the electron clouds will be collected on the pads being read out and the signal-to-noise ratio will be lower.

The same measurements were also done with a single normal pad ($6 \times 15mm^2$). The result is shown in figure 4.7. Again it is clear that the reso-

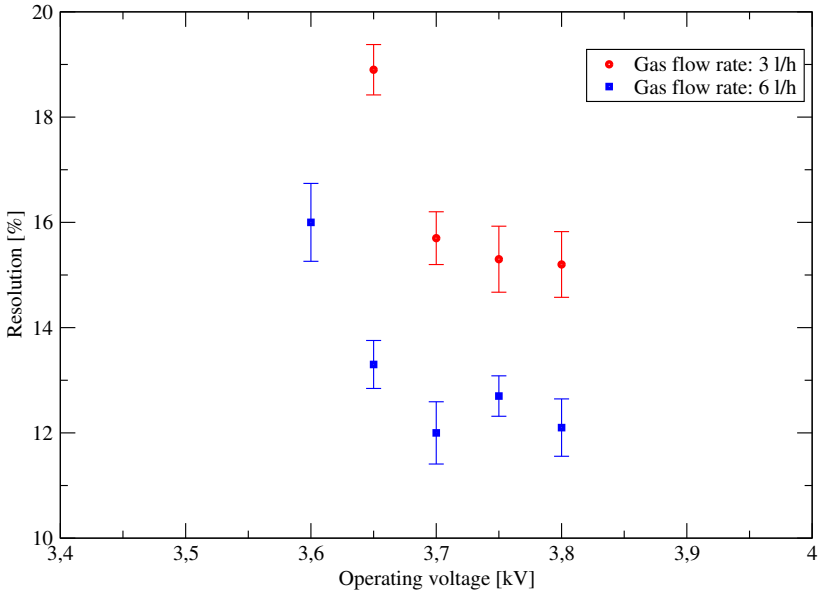

Figure 4.5: Plot of the relative energy resolution of 5.9 keV photons at different gas flows and different voltages. The measurements were done with the large pad ($27 \times 27mm^2$).

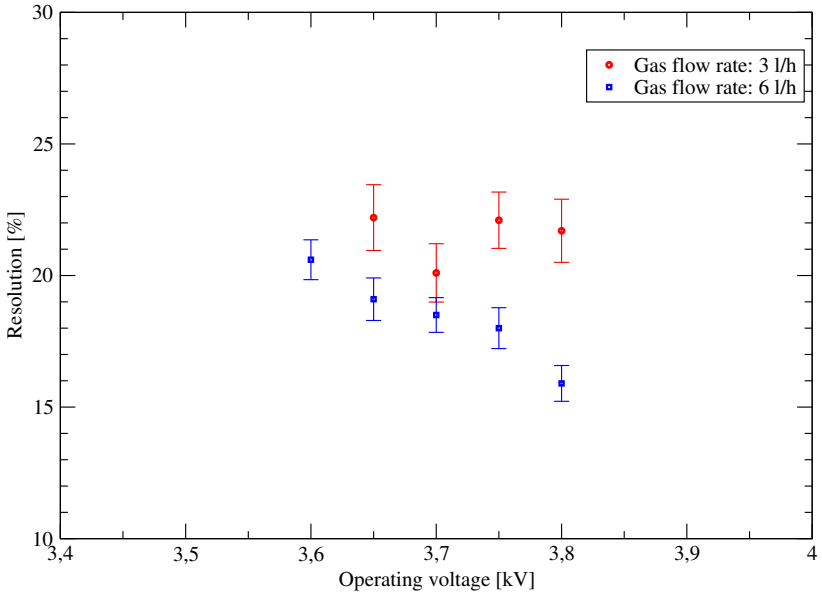

Figure 4.6: Plot of the energy resolution of the 5.9 keV photon peak at different gas flows and different voltages. The measurements were done with three $6 \times 15mm^2$ pads connected together.

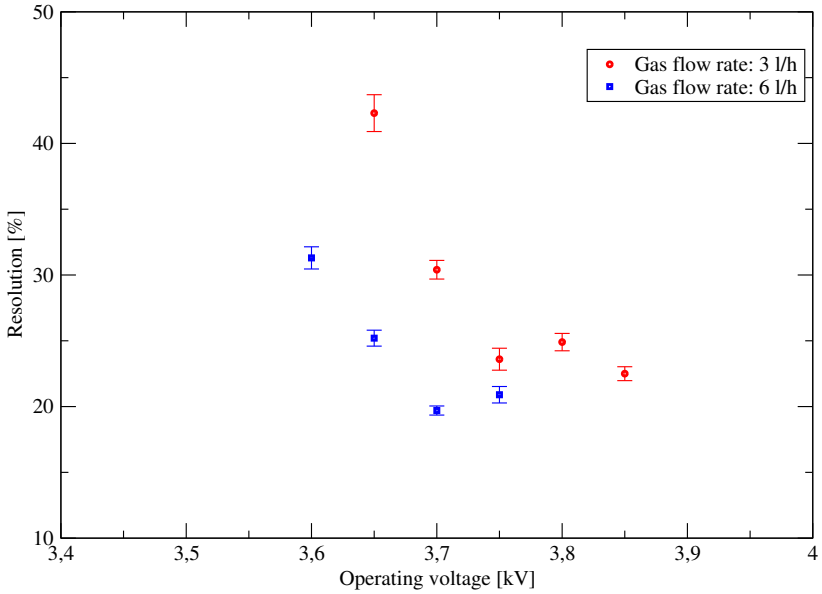

Figure 4.7: Plot of the relative energy resolution of the 5.9 keV peak at different gas flows and different voltages. The measurements were done with a single normal pad ($6 \times 15mm^2$).

lution is even worse due to an even smaller read out area.

The energy resolution will not be this low or lower for the ALICE TPC even though the $6 \times 15mm^2$ and smaller pads will be used in the ALICE TPC. The whole electron cloud will be collected by several pads together since they are laying close to each other. The combined signal from several pads will therefore determine the energy loss of one particle.

It is clear from all of the measurements that a high gas flow through the detector gave a better resolution. As for the higher gain at higher gas flow rates, this is probably due to variation in the oxygen level in the detector. The losses of charges to oxygen molecules give a broadening in the spectrum which lead to a lower resolution. This shows that the purity of the gas is important when operating the detector.

Measurements with the largest pad gave best resolution while measurements with the smaller pads gave worse resolution. Electron avalanches will only be partially collect on the readout pad making a broader spectrum and lower resolution.

The relative resolution measured with the prototype GEM detector is poor compared with other chambers. There was previously a GEM detector with three foils with only standard pitch size (140 μm) (denoted S-S-S) at the Department of Physics and Technology at the University of Bergen. A previous master student used this chamber and measured the relative resolution for 5.9 keV photons from a Fe-55 source at gain of 2000 to be 8.8

% and 9.7 % with a $30 \times 30mm$ pad and a $6 \times 15mm$, respectively [12]. This is much better than the results obtained with the GEM prototype. The reason for this is that the S-LP-LP-S foil configuration and the voltages at each foil and field is used to minimize the ion back flow and not to optimize the energy resolution. The large pitch sized foils and a low voltage on the two first GEM foils make sure that only a small amount of positive ions drift back into the TPC volume and distort the electric field. Figure 4.8 shows that it is not possible to have both optimal resolution and low ion flow back. The ion back flow requirements for the ALICE TPC is having $< 1\%$[3]. Low ion back flow has high priority at the ALICE TPC since distortions of electric would distort the drift time of electrons and reduce the tracking performance which is the main task for the TPC.

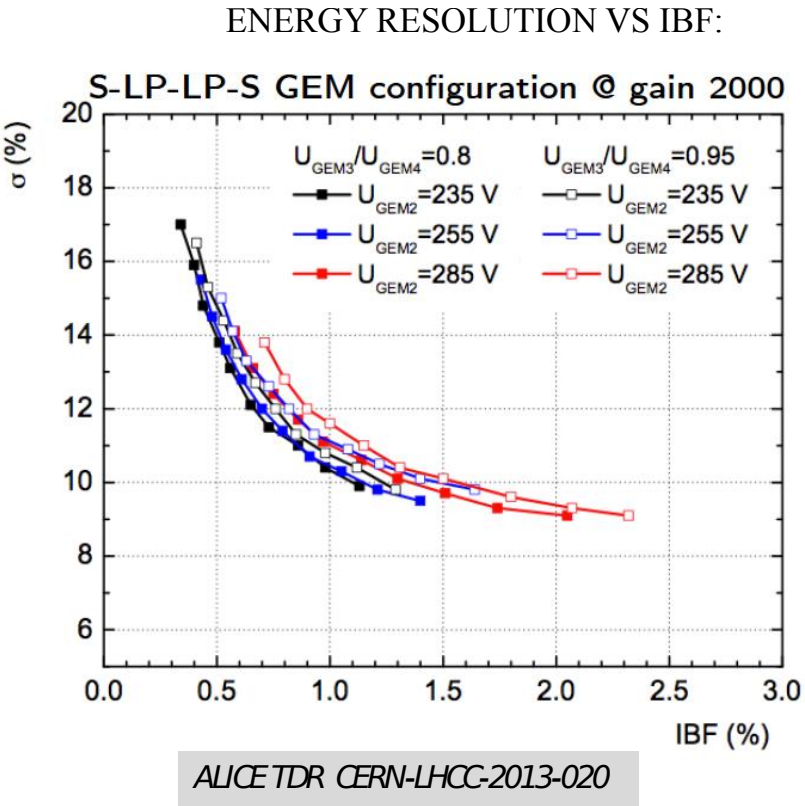

Figure 4.8: The energy resolution as a function of ion flow back measured for ALICE TPC [3].

4.3 Comparison of different pads

The size of the pads are linked to the size of the electron avalanche or often called the cluster size. The cluster size in the ALICE TPC will be about

2 cm^2 and is therefore larger than the readout pads [3]. If a cluster is only collected on one pad the position resolution is determined by the pad size and in order of a cm. If the cluster is shared between the several nearby pads the signal from the different pads can be weighted and the resolution is improved to be much better than the pad size.

The energy spectrum from the Fe-55 source was measured using all the different pad sizes. The detector was operating at about 2000 gain in the argon gas mix used previously. The spectra was fitted to find the mean and sigma of the main peak of the energy distribution. The results are showed in table 4.2. The position of the peak varies a lot from about 2100 to 5100. The smaller pads are clearly not able to collect all the charge created by the photons meaning that the cluster size is larger than at least 6×15 mm^2. The peak measured with the 6×15 mm^2 and 27×27 mm^2 pad was at channel 4338 and 5064. This means that peaking amplitude measured with the $6 \times 15 mm^2$ pad is 85 % of the peaking amplitude measured with large pad (27×27 mm^2). It seems that the 6×15 mm^2 pad collects a large part of the total charge created.

Pad size	Mean	Sigma
4×7.5 mm^2	2091	1247
6×10 mm^2	3204	1316
6×15 mm^2	4338	1161
27×27 mm^2	5064	914

Table 4.2: The mean and sigma of the main peak in the energy spectrum from a Fe-55 photon source measured with different pads.

Chapter 5

Measurements with minimum ionizing particles

The GEM detector prototype was also tested using a high energy beta source where the primary goal was to test the detector with minimum ionizing particles (MIPs).

The radioactive source strontium-90/yttrium-90 was used during these measurements. Sr-90 decays by beta decay by emitting an electron with an energy up to 0.546 MeV. The half life is 28.79 years. The decay product of Sr-90 is yttrium-90 which also decays through beta decay. The maximum energy of the emitted electron is 2.28 MeV and the half life is 64 hours for Y-90. Zirconium-90 is the daughter isotope of Y-90 and it is stable. The activity of the source was about 1.14 MBq.

In a beta decay the electron and the anti-neutrino shares the total decay energy in varying degree. Due to this electrons most often have lower energy than maximum decay energy. In this experiment this means that most of the electrons have a low energy and are not MIPs. Only the electrons with energy above about 1 MeV and below about 5 MeV can be considered as minimum ionizing particles. In order to only measure the MIPs an external trigger was used to discriminate the low energy electrons and the MIPs.

In the energy range from some keV to some MeV electrons lose their energy through ionization and excitation. At higher energies bremsstrahlung dominates and at lower energy other effects like electron capturing becomes relevant. The energy loss through ionization and excitation is described in chapter 2. When the energy loss is at the minimum the particles are called MIPs. Since the ionization of the traversed medium is small the signal in detectors like the GEM prototype is small.

Since the signal from MIPs is small it is especially important to reduce the noise of the system. The signal amplitude was just above the noise. As seen in figure 5.3, the SAMPA chip carrier board was therefore connected directly to the readout pin without any cable in order to reduce the noise.

5.1 Measurements without external trigger

The detector was first tested without the external trigger, only a software trigger in the LabView program.

The experimental setup was the same as used for the gain and resolution measurements of the detector, only the radioactive source was different. The gas used for this experiment was the $Ar + CO_2(90 + 10)$ mix at a gas flow rate of 3 litres per hour. This setting was found to give gain of about 2000 as seen in section 4.1. The large pad was read out. There was little point of doing the measurements with the smaller pads because of the low resolution and even smaller signal amplitudes.

To set the right threshold of the software trigger the noise was measured. Like figure 5.1 shows the noise was below 300 ADC channel (37.5 mV) in the pulse height histogram so 300 was used as the threshold for the measurement.

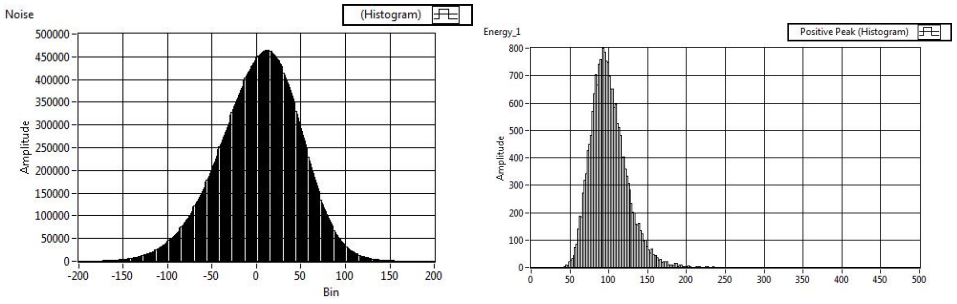

Figure 5.1: To the left is the histogram of the noise where the base line fluctuations of the signals are filled into the histogram. The noise is about 50 ADC channel. To the right is the pulse hight spectrum of the noise showing that noise was up to about 200 ADC channel. 300 was ADC channel was set as threshold.

The energy spectrum from both the source and the background is shown in figure 5.2. MIPs should make a Landau energy distribution when traversing a thin sensitive detector volume. Figure 5.2 shows that this is not the case. The spectrum does not provide any information about the MIPs. It only shows that the radioactive source gives us a lot of signal with all kinds of different energies. Since the electrons have all energies up to 2.28 MeV it is not possible to tell how much energy the electrons at a given energy deposit.

This measurement also shows that using a beta source for discharge studies is not effective. The electrons deposit little energy in the detector giving few signals with high amplitude even at gain of 2000.

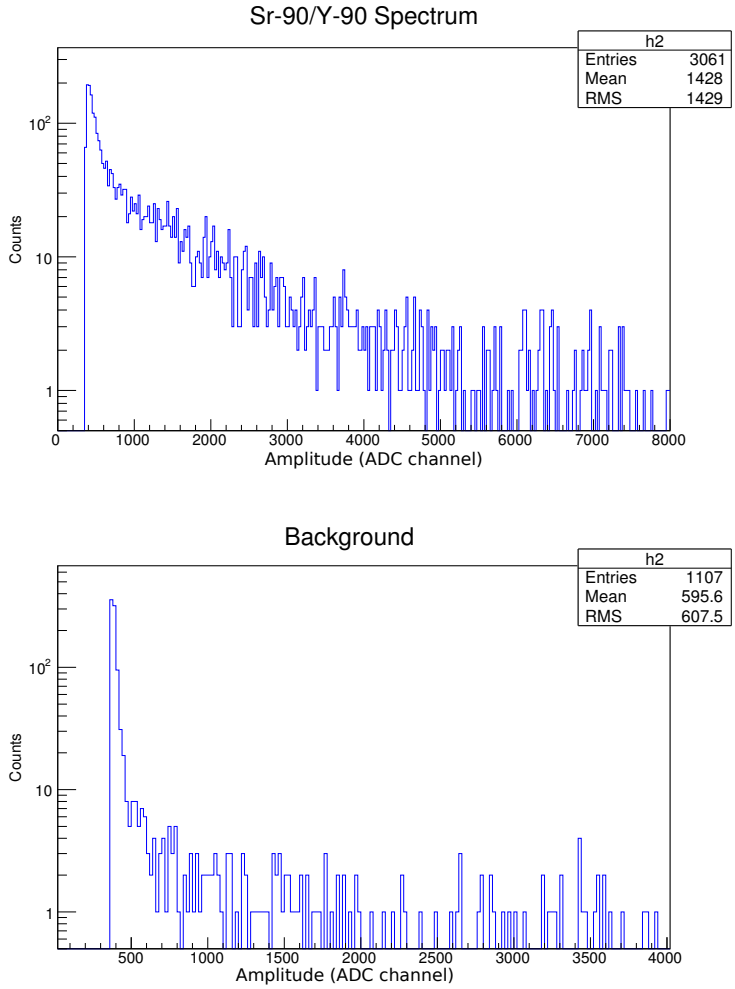

Figure 5.2: The pulse height spectrum from the source is shown at the top. The pulse height spectrum of the background at the bottom. Both spectra are measured with software trigger.

5.2 Measurements with external trigger

In order to measure MIPs an external trigger was used to only measure the electrons of high energy from the Sr-90/Y-90 source.

A plastic scintillator was placed directly below the source and the large pad which was read out. Only the electrons of high energy will reach the scintillator as they pass through the detector as minimum ionizing particles. The low energy electrons will be stopped in all the material between the source and the scintillator. The signal from the scintillator was send to a discriminator. The discriminator was set to have a threshold correspond to

1 MeV electrons. This means that only signals corresponding to electrons with energy of about 1 MeV and above were send to the data acquisition system and stored. It is assumed that electrons lose approximately all their energy in the plastic scintillator since the range of 2.28 MeV electrons is only about one cm in plastic and the energy of electrons is not that high when hitting the plastic scintillator since the electrons have already passed through a lot of material.

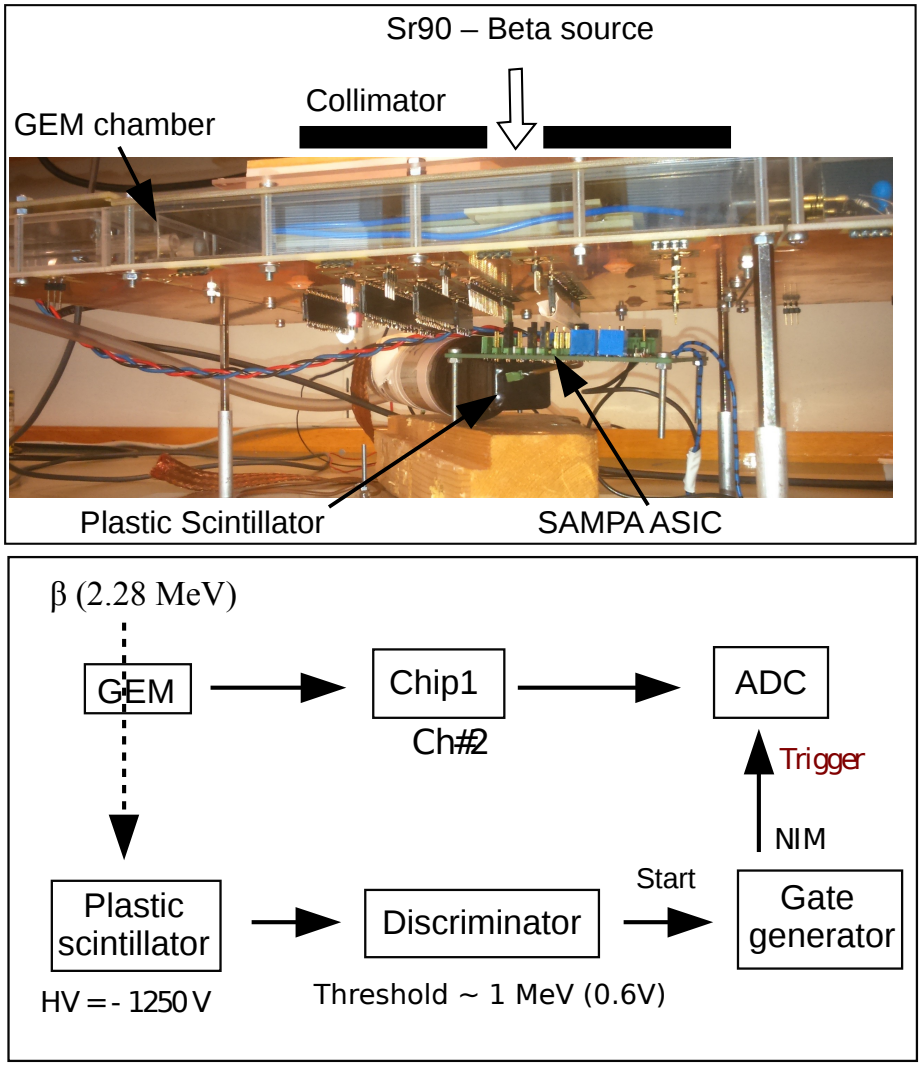

Figure 5.3: The top picture shows experimental setup. The readout chip was directly connected to the readout pin and the plastic scintillator was placed beneath the SAMPA carrier board. The bottom figure shows the trigger schematics. The signal from the scintillator was fed to a discriminator with threshold of about 1 Mev.

The threshold was selected from measurements of the highest amplitude the beta source gave when radiating the plastic scintillator. The highest value corresponds to the 2.28 MeV electrons. Approximately half of this value was used as threshold which means that only signals from electrons above roughly 1 MeV was stored.

The first measurement was done with operating voltage of 3.8 kV and gas flow of 3 litres per hour with the $Ar - CO_2(90 - 10)$ gas mix. As seen in section 4.1, this means that the gain was about 2000.

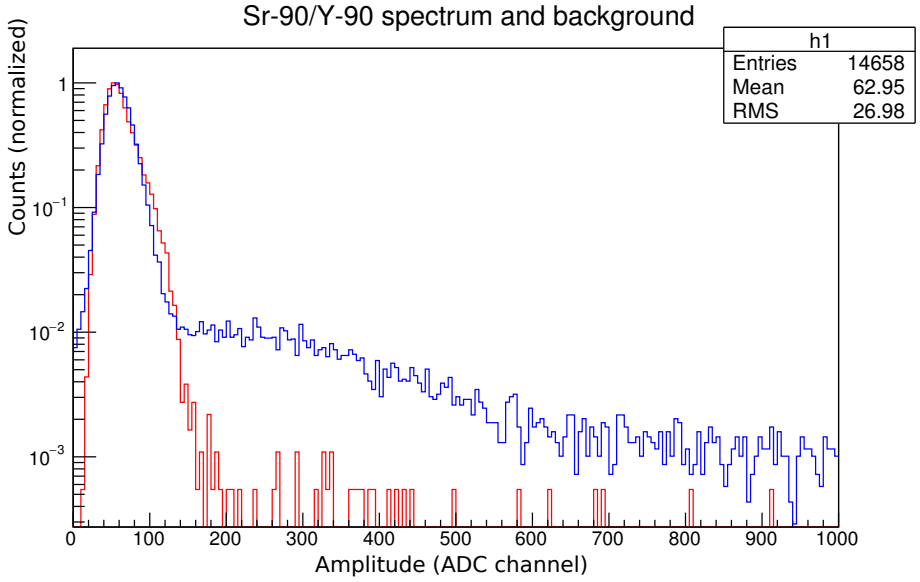

Figure 5.4: The blue line shows the normalized spectrum from the strontium-90/yttrium-90 source while the red line shows the normalized background and noise. Both spectra are measured with the external trigger at 2000 gain.

Figure 5.4 shows the normalized result of measurement with the beta source and the background. Maximum counts for the beta spectrum was 6919 while the maximum counts for the background spectrum was 1828 with a bin size of five. The normalization is done in order to compare the two spectra even with different number of counts.

The blue line shows the spectrum from the S-90/Y-90 source with the external trigger while the red line shows the background and noise also measured with the same setup. The large leftmost peak is noise and the maximum noise is up to about channel 180 (22.5 mV) of the DAQ-system which means that almost everything above is signals from the source.

The signal amplitude are as expected low since it is minimum ionizing particles measured in a thin sensitive volume of a gas detector. The signal for most of the counts is just above the noise. The spectrum from the source is expected to be a Landau distribution. This is not clear from this

measurement. The most probable value of the distribution is not clearly distinguished from the noise and it seems to be to many counts at higher amplitude. A larger drift gap or higher gain would probably shift the spectrum to the right so that the most probable value of the Landau distribution would be clear.

The measurement was repeated with a higher gain in order to clearly see the expected Landau distribution. The noise was not expected to increase much since it was mostly noise from the electronics and not related to the gain of the chamber. The setting was the same as previous except that the voltage was increased to 3.9 kV which means that the gain was roughly about 2500. The spectrum from this measurement is shown in figure 5.5.

As expected the noise did not increase much with the increased gain. The Landau distribution from this measurement is clearly visible with the most probable value about channel 244. The histogram was also fitted using root. Figure 5.6 shows that it gave a good fit for the range form about 200 to 700 but it still was to many counts at higher amplitudes.

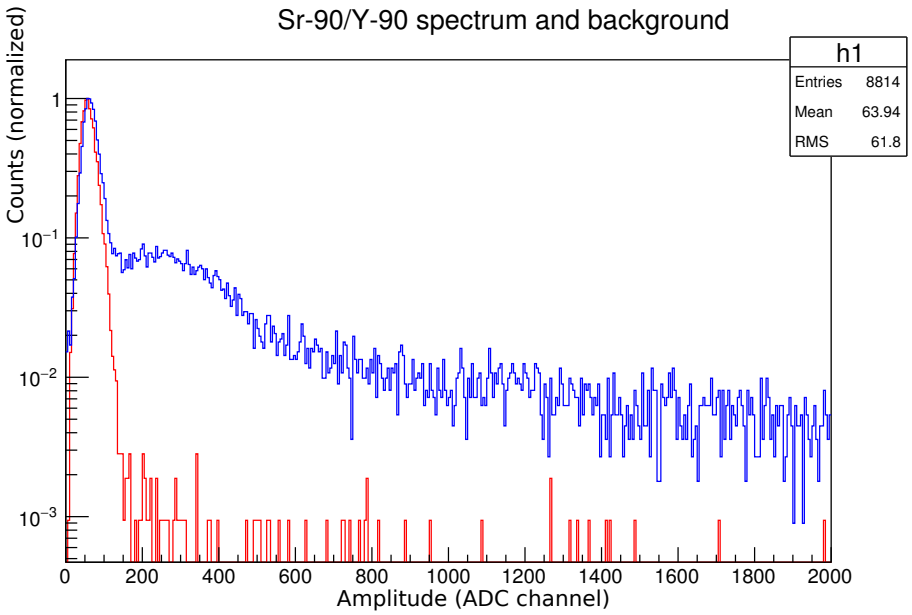

Figure 5.5: The blue line shows the normalized spectrum from the strontium-90/yttrium-90 source while the red line shows the normalized background and noise. Both spectra are measured with the external trigger at 2500 gain.

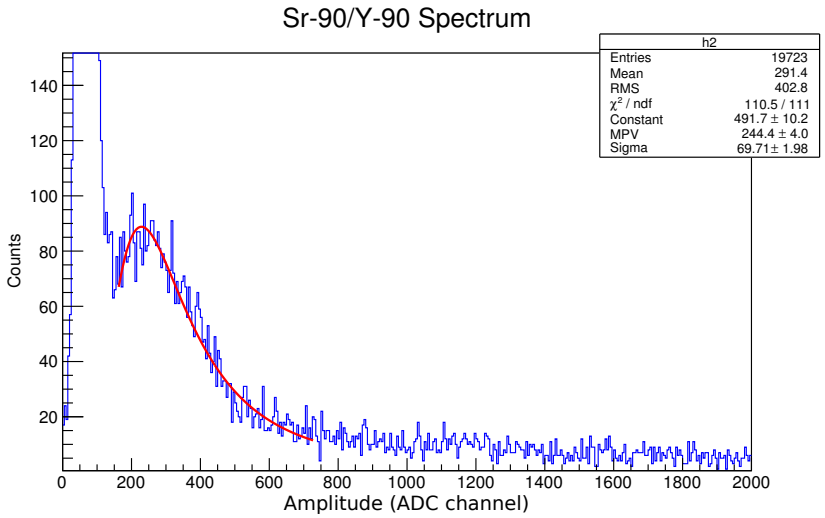

Figure 5.6: The solid red line shows that a Landau distribution fits well with the Sr-90 spectrum energy.

Chapter 6

Measurements with various alpha sources

6.1 Measurements with an external alpha source

The GEM detector was also tested with an external alpha source to see how the detector responded to heavily ionizing particles. An Am-241 source with an alpha energy of 5.5 MeV was used. The source also emits a 59.5 keV photon. The activity was about 34.7 kBq. Alpha particles have a short range and are easily stopped. The source was placed close to a thin polymer window in the detector and was pointing at the pad being read out. This setup can be used for discharge studies. The discharges will then be localized only to the small area irradiated by the source.

The high voltage settings needed to be different than for photon and beta measurement while doing measurements with an alpha source. Alpha particles are heavily ionizing and deposit a lot more energy in the detector compared with X-rays and the beta radiation from Fe-55 and Sr-90. The data acquisition system could not handle signal of more than 1 V or differential signal of 2 V from the SAMPA readout chip. The detector need therefore to be run at very low gain of less than 1000. The operating voltage used to achieve was about 2.9-3.15 kV compared to the voltage of about 3.6-3.8 kV used to detect 5.9 keV photons

The signal from the alpha source became piled up because of the high rate as shown in figure 6.1. The integral of the pulses were therefore saved in addition to the maximum peak value. The rate was reduced when collimators were used which also reduced the pile-up.

6.1.1 Collimator study

Measurements with the alpha source both with and without collimator were done in order to understand the spectrum and reduce the energy spread.

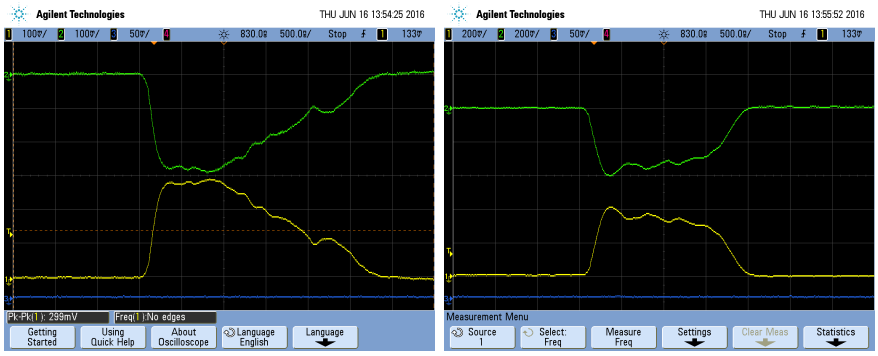

Figure 6.1: The alpha pulses piled up because of the high rate. The figure shows two examples of how the differential pulses from the detector looked like.

Measurements without collimator, with a 1 mm collimator and with a 0.5 mm collimator where done. The collimators were aluminium foil with a hole. Every parameter in the measurement where kept the same except for the collimator.

The measurement was performed in with two different operating settings. At first it was performed the gas was $Ar + CO_2(90 - 10)$ at a flow rate of 3 litres per hour. The signal was read out using a $6 \times 15mm^2$ pad. The measurements were also performed in the $Ne-CO_2-N_2(90-10-5)$ gas mix also at flow rate of 3 litres per hour. Three $6 \times 15mm^2$ pads were connected together and read out. The operating voltage was 3.10 kV in both cases. Both settings gave very similar results.

The source was placed on one of the thin windows which made the source point at the pad being read out. The signals were saved using LabVIEW [13]. Both the peak values and the integral values of the peaks were saved.

First it is important to note that all the signals in the spectrum come from the Am-241 source. The signal disappeared completely if the source was lifted away from the detector so that it was a gap of about 5-10 cm between the source and the detector. The gain of the detector was to low to get signals from other particles than alpha particles. The noise of the system was well below the left peak in figure 6.2 and 6.3.

The right peak comes from alpha particles that hit the detector with an angle of about 90 degrees and therefore ionizing a lot above the pad being read out. This gives the peak at large amplitude. The left peak seems to be strongly reduce when a collimator is used. This may suggest that the pulses giving rise to the lower peak come from alpha particles which not hit the detector with an angle of 90 degree. The use of collimator stops most of the particles with inclined trajectory and number of signals at lower amplitude compared to the main peak.

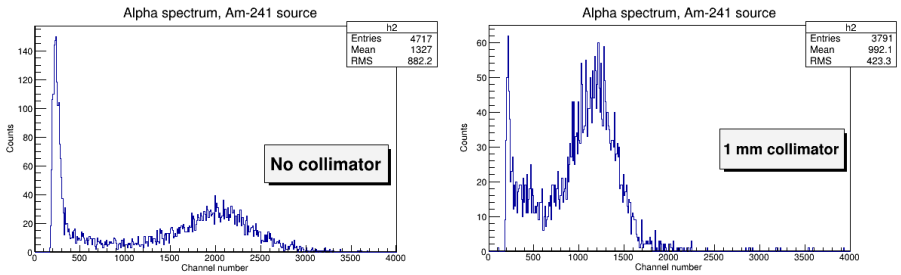

(a) No collimator (b) 1 mm collimator

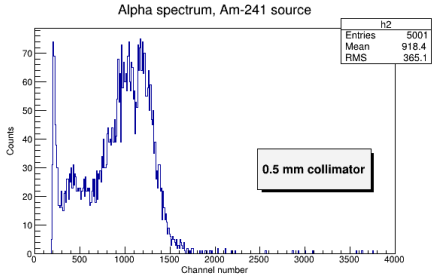

(c) 0.5 mm collimator

Figure 6.2: Histograms of the alpha energy spectrum measured in $Ar - CO_2(90 + 10)$ with and without collimator. One $6 \times 15mm^2$ pad was read out.

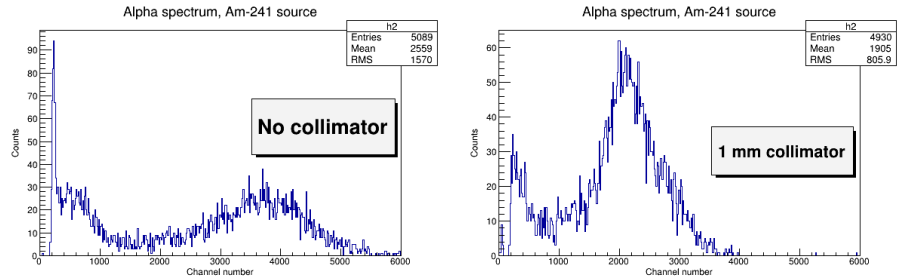

(a) No collimator (b) 1 mm collimator

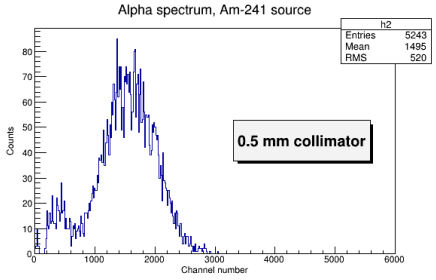

(c) 0.5 mm collimator

Figure 6.3: Histograms of the aplha spectrums measured in $Ne - CO_2 - N_2(90 - 10 - 5)$. Three $6 \times 15mm^2$ were connected together and read out.

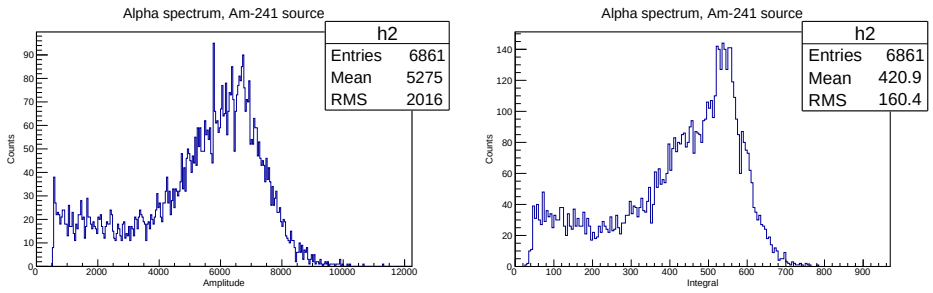

Figure 6.4: To the left is the pulse height spectrum of the piled-up alpha pulses. To the right is the histogram of the integrals. The voltage for this measurement was 3.10 kV.

The main peak also shifts to the left when a collimator is used. This occurs since the rate is reduced in the collimated cases and we do not get as many pulses piled up and therefore lower amplitude. The region between the peaks may come from electron clouds that are only partially collected on the pad being read out and therefore gives signals with varying amplitude.

6.1.2 Energy resolution

The alpha energy spectrum from the Am-241 source was also measured at different voltages. A 0.5 mm collimator was used to reduce the rate and the pile-up of pulses. The usual data acquisition system was used. In addition to only save the maximum amplitudes, the integrals of the pulses were saved. This was done since the pulses were piled up. The integral value corresponds to how much charge that was collected. Histograms of the pulse height and the integrals are shown in figure 6.4.

The shape of both spectra are similar to each other but the spectrum of the integrals does not fit well to any known distribution. The peak of the pulse height spectrum is roughly a Gaussian distribution. The peak corresponds to how much energy the alpha particles lose in the drift region of the detector. The energy resolution of this peak was found at different voltages. This is not the resolution of the energy loss of a single alpha particle since the pulses still with the collimator were a little piled up. The main peak was fitted by a Gaussian distribution and the mean and the sigma was found. The results are shown in figure 6.5.

This shows that this kind of setup for discharge testing seems to give a well defined energy spectrum but the pile-ups are probably worsen a more well defined energy spectrum of single alpha particles.

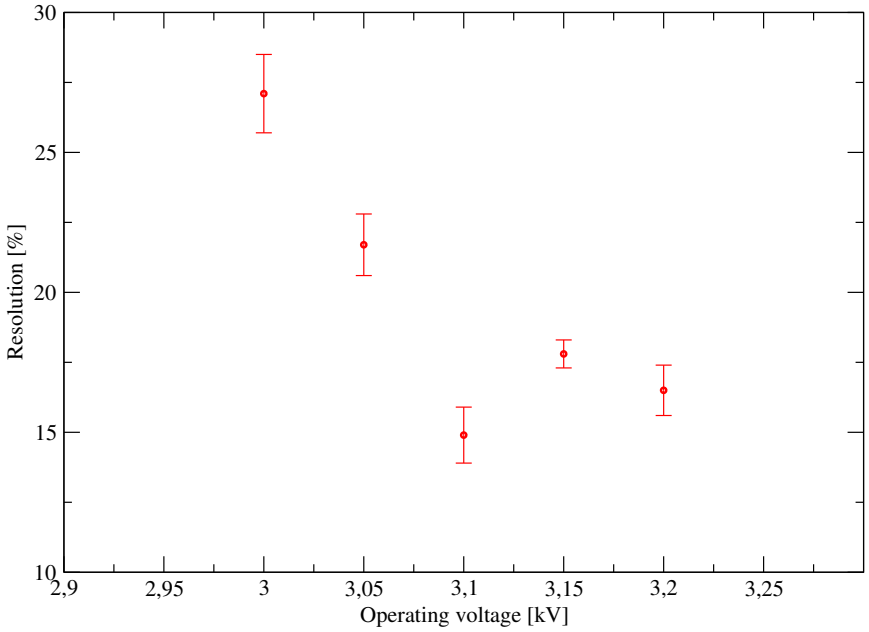

Figure 6.5: Plot of the energy resolution of the piled up alpha pulses from a Am-241 source. The measurements were performed in the neon gas mix. One $6 \times 10mm^2$ pad was used.

6.2 Tests using radon sources

The GEM detector prototype was also tested using a radioactive gas, radon-220, as a source. Radon gas from a rock and gas mantles, both containing thorium, was added to the gas flow and flushed into the chamber. This will give radon decaying in the whole gaseous volume of the detector. Rn-220 is an alpha emitter and will therefore create a lot of charge when decaying. This will make the conditions for discharges more similar to actual large experiments like the ALICE TPC than using an external alpha source.

The rock was found in a local Norwegian mountain where the natural abundance of thorium is high. A gas lantern mantle is glowing and makes a bright light when heated by a gas flame. Many gas mantles are enriched with thorium and are commercially available. Ten thorium gas mantles were used as a source.

6.2.1 Thorium decay chain

The thorium decay chain starts with naturally occurring isotope thorium-232 with a half-life of 1.4×10^{10} years. As shown in figure 6.6, Rn-220 is the sixth daughter isotope and the only isotope which is a gas. This gas can be used as a radioactive source for a gaseous detector like the GEM detectors when added to the gas flow. This can be done by placing some material

containing thorium in the gas flow before the gas are entering the detector. The radon gas will be transported to the detector together with the rest of the detector gas.

Rn-220 is a alpha emitter and has a half-life of 55 seconds. A lot of the radon in the gas flow will decay in the detector giving rise to a signal that can be read out. Figure 6.6 shows that Rn-220 is a gas while the isotopes after radon-220 in the chain are solids and also radioactive. This means that daughter isotopes after radon have decayed will not be flushed out of the detector with the gas flow but stay in the detector and possible give more signal of many kinds in the detector. However the gain was kept low for these measurements because of the heavily ionizing alpha particles so that gain is too low to measure beta and gamma radiation.

Another consequence will be that some radioactive material will stay in the detector after the gas containing Rn-220 is turned off. This means that it takes some time before the chamber is clean and ready to use with other sources or for background measurements. The half-life of 10.6 hours of Pb-212 can be use as a guideline for the activity after the radon is turned off since this isotope has the longest half-life in the chain after Rn-220. The other isotopes have much shorter half-life.

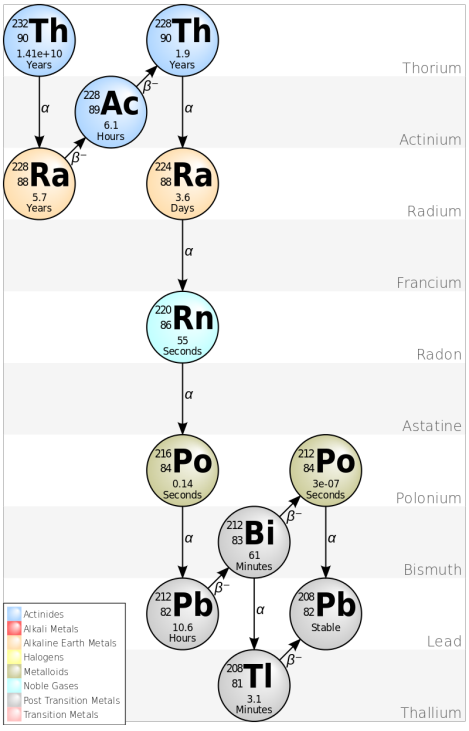

Figure 6.6: Schematic of the thorium decay chain [11].

6.2.2 Experimental setup

A rock with a high natural abundance of radioactive material and thorium mantles were used as sources of radon gas. The rock was kept in a air tight chamber. The gas could be flushed through this chamber if measurements with the radon gas was to be done. Otherwise the chamber containing the rock could be bypassed. Two photographs of this is shown in figure 6.7. A nearly identical setup was used for measurement with the thorium mantle as seen in figure 6.8. Ten thorium mantles was place in a cylindrical container were the gas was flowing through. This could also be bypassed.

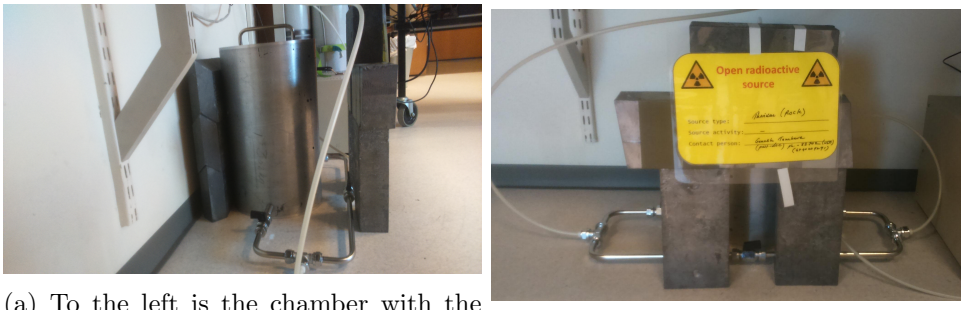

(a) To the left is the chamber with the rock and to the right is the pipe used when the rock is bypassed.

(b) Front view of the gas system with some shielding in front of it.

Figure 6.7: Photos of the gas system for measurement with the rock and the mantles.

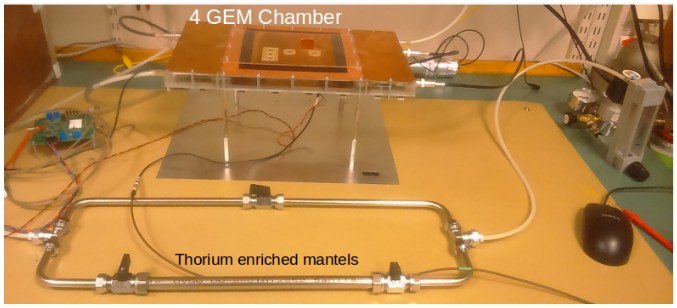

Figure 6.8: Photo of the gas system used for measurement with the mantles.

When measuring with the radon sources it was desirable to read out a large area of the anode readout plane. This would give a higher rate and readout more of the ionization created by one alpha particle. Reading out only a small area would only give a small fraction of the ionization created. This was hard to do since reading out a large area means that the capacitance of the input of the SAMPA chip would be large and therefore increase the noise a lot. It also made the SAMPA chip oscillate. Other preamps than the SAMPA chip was also tested if they could handle the high capacitance

better but the noise was still high so the SAMPA chip connected to the large pad was still used.

This experimental setup can be used for discharge studies if in addition the voltage on the last GEM was measured.

6.2.3 Results using the rock as source

The first measurement with the rock was done with the large pad ($27 \times 27mm^2$) in the argon gas mix with a gas flow of 2 litres per hour. The operating voltage was kept low at 2.9 kV. At this setting only alpha particles are expected to be detected due to the low gain of the GEM detector. Cosmic particles and beta particles and photons from the radioactive source are not expected to be seen since the ionization in the sensitive volume of the detector is not enough to give detectable signals. The noise was also high because of the high capacitance of the large pad making it even less likely to see signals from other radiations than the heavily ionizing alpha particles. All of the following measurements with the rock were performed for 2.5 hours and the maximum amplitudes of the signals were stored.

Measurement with the Rn-220 in the gas flow was first done. The gas flow with the source had been for a few hours before the measurement was done order to get a build up activity of daughter isotopes and stable activity in the detector. The result of this measurement is shown in figure 6.9

Just after the measurement with the radioactive source in the gas was done a new measurement was done with rock bypassed. The rock had then been bypassed for about one minute(approximately the half-life of Rn-220). In addition the gas was still flushing through the detector without the source so the amount of alpha decays from the radioactive gas was expected to be low. This was done in order to measure the radioactive decay product from the radon gas. The signal rate when the measurement started seemed to be almost as high as before the rock was bypassed and was clearly lower some minutes after the measurement was started. The measurement was done for 2.5 hours and the rate was clearly reduced at the end of the measurement. The result is shown in figure 6.10.

A measurement of the background was performed roughly 22 hours after the rock was bypassed. This mean that the longest lived isotope had gone through more than two half-lives before the measurement was done. Some alpha pulses from the last part of the decay chain may have been recorded. This is shown in figure 6.11.

The peak around channel 900-1000 did not come from the radioactive source but was noise from an unknown source and will be discussed later.

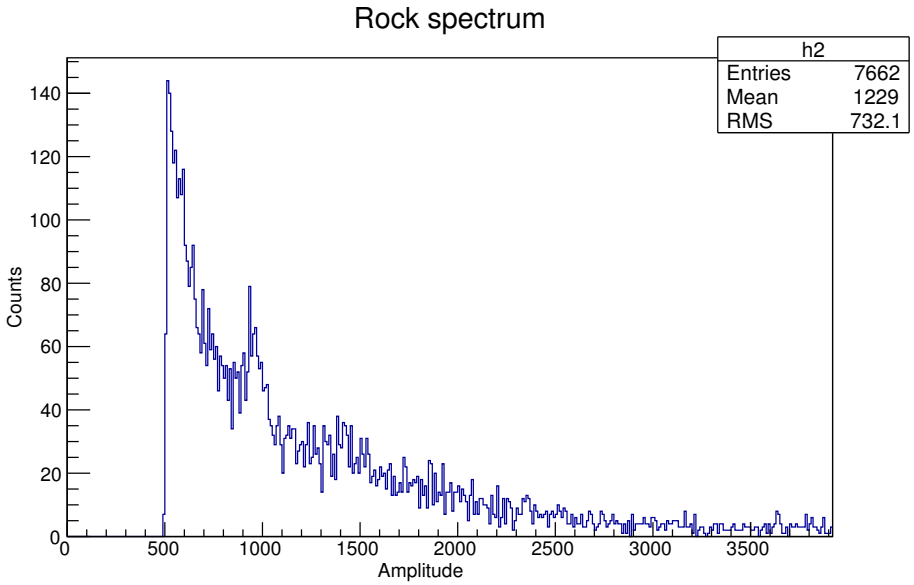

Figure 6.9: The spectrum measured from the radioactive gas from the rock.

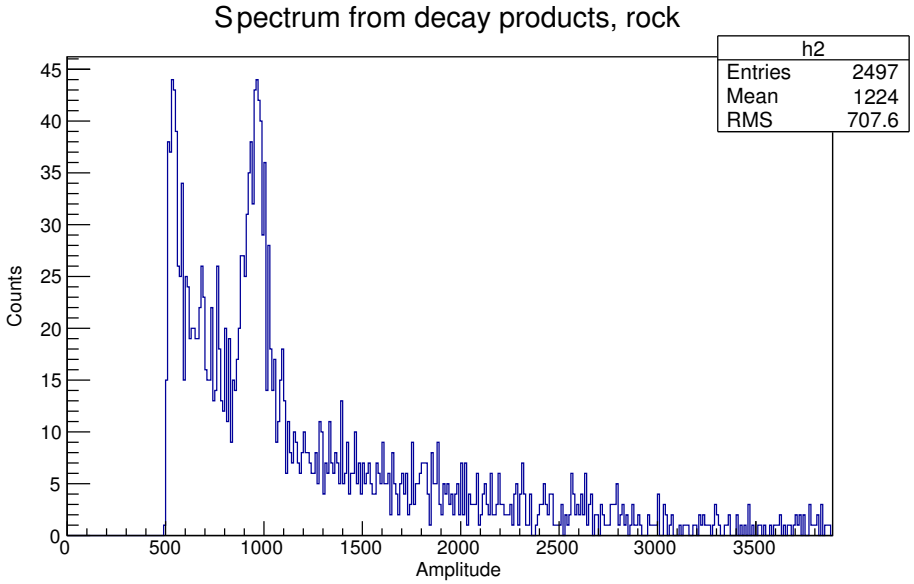

Figure 6.10: The spectrum measured right after the radioactive gaseous source was turned off. The signals mainly come from the part of the thorium decay chain after Rn-220.

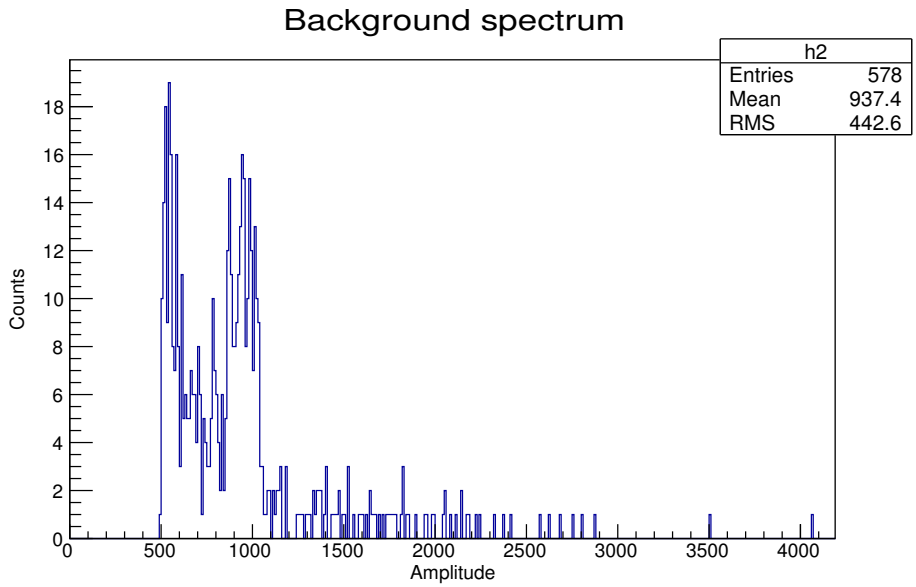

Figure 6.11: This is the pulse height spectrum of the background.

6.2.4 Results thorium mantle

The spectrum from the ten mantles was measured in the same way as for the rock. The settings were the same meaning the large pad was read out. The argon gas mix was used at a flow rate of 2 litres per hour. The operating voltage was 2.9 kV. The counting time was two hours for all the measurements with the mantles.

The background spectrum was measured first several days after last time a gaseous source was used which mean that the contribution of the last part of the decay chain was approximately zero. The background spectrum is shown in figure 6.12.

The spectrum of the radon from the mantles was then measured after the source had been on for one hour. The result is viewed in figure 6.13. The spectrum is very similar to the spectrum from the rock shown in figure 6.9.

The thorium mantles were then bypassed and a new measurement was done in order to measure the decay products of radon. The result is viewed in figure 6.14. The rate seemed to be almost as high as with the source in the gas flow in the start of the measurement. At the end of the measurement the rate was clearly reduced.

The noise from an unknown source still gave a peak around 900-1000 ADC channel. This will be further discussed in the next section.

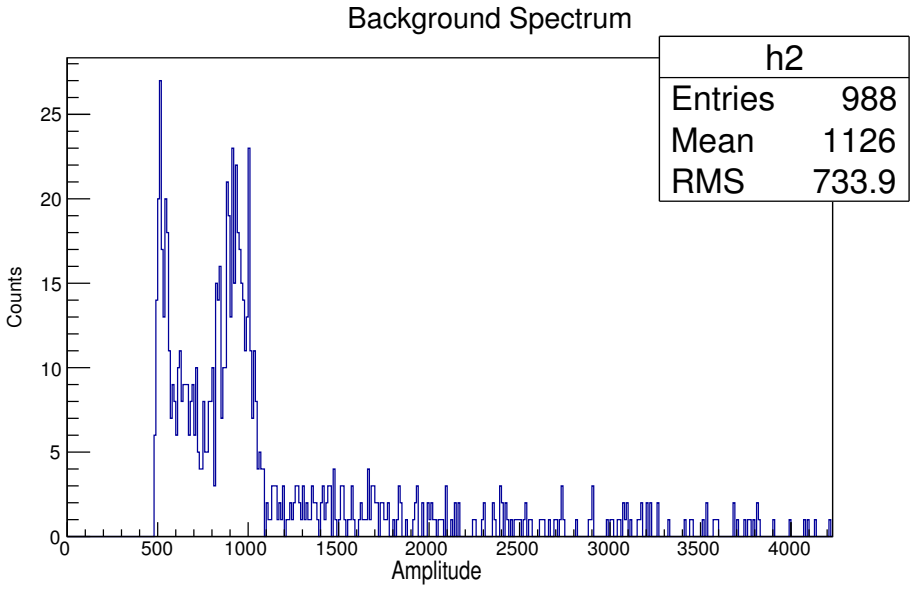

Figure 6.12: This is the background spectrum measured for two hours.

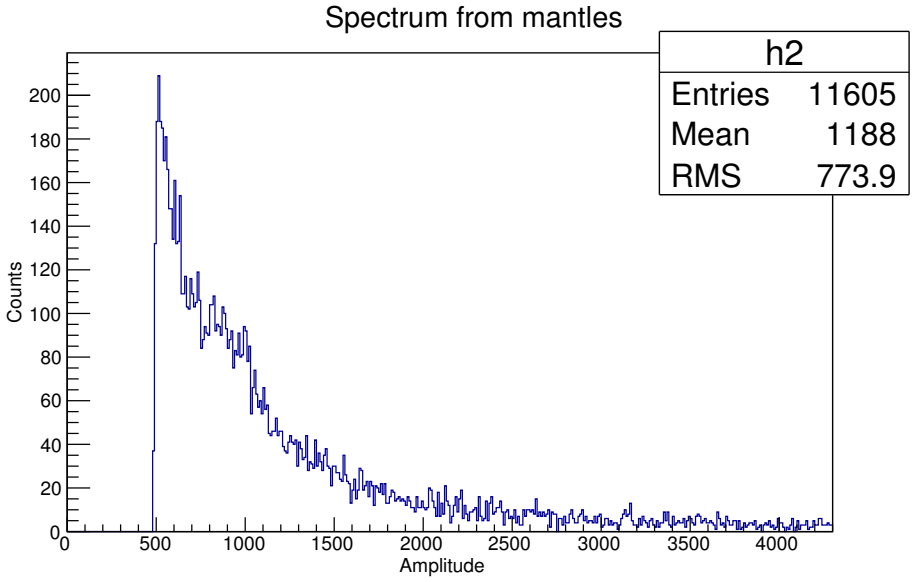

Figure 6.13: This is the spectrum from the Rn-220 from the thorium mantles measured for two hours.

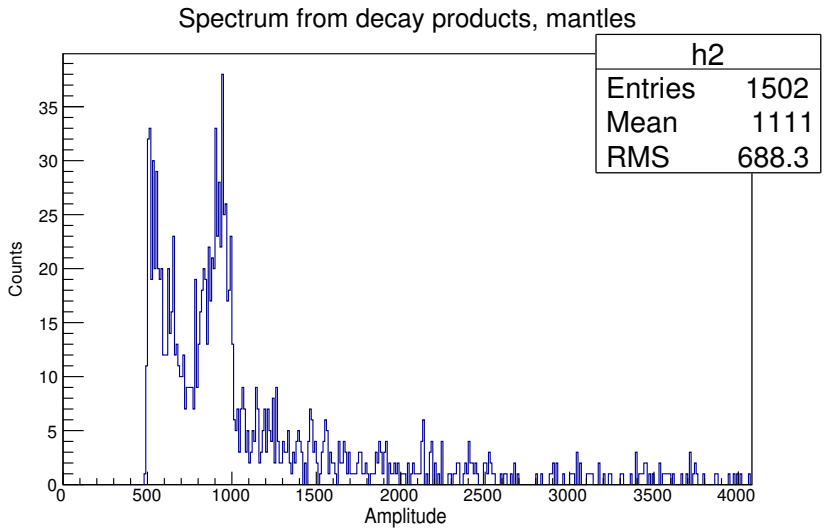

Figure 6.14: This is the spectrum from the decay products after the supply of radon was turned off. It was measured for two hours.

6.2.5 Discussion of the measurements with the rock and the mantles

The shape of the spectra measured form the mantles and the decay chain of the mantles are very similar since the signals mainly come from a radioactive gas emitting alpha particles and alpha particles emitted from the daughter isotopes.

There were some problems with some unknown noise wile doing measurements with the rock and the mantles. The noise gave a clear peak around channel 900 to 1000. Signals with other amplitudes were also seen but they were a lot rarer. These were not signals from the radioactive source or the background but the origin of these signal was not determined. The signals occurred even if the high voltage supply of the detector was turned off but at a lower rate than if the high voltage was one. The signals were not seen when only the SAMPA chip was connected to the DAQ system or an oscilloscope meaning that the signals did not come from the SAMPA chip alone. The signals seemed therefore to be created in the detector even if it high voltage supply was turned off.

These noise pulses were easy to distinguish from regular pulses because of the pulse shape. A typical pulse shape is shown in figure 6.15. The signals had a characteristic large drop before an amplitude usually about 900-1000 ADC channel. Some rare pulses with amplitudes of some thousands were also observed.

The rate of these noise pulses to happen was not straight forward to determine because the rate seemed to be dependent on the operating voltage

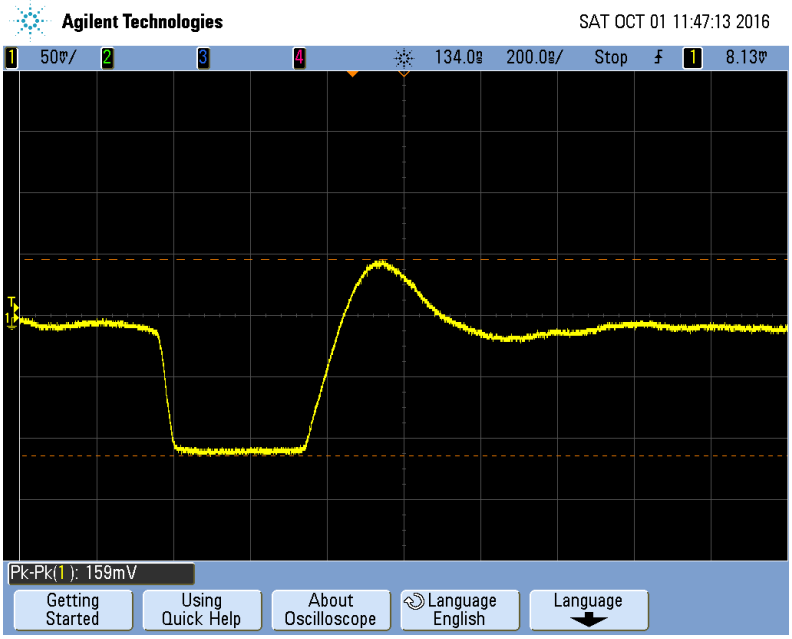

Figure 6.15: Unknown noise appeared during the experiments with the rock and the mantles.

and maybe of the actual rate of signals in the detector. The rate was measured to be in the order of 0.1 Hz when the source was used and it seemed to be a bit lower if there was no source. This is much lower than the activity of the source. The contribution to energy spectrum from the noise at different amplitudes than around 900-1000 ADC channels was therefore neglectable.

The measurements with the rock and the mantles show that radioactive material is transported with the gas flow into the detector giving a lot of signal. The emitted particles must be alpha particles since they are detected in the detector at low gain. When the radioactive source is bypassed there are still a lot of activity in the detector. This have to come from daughter isotopes of the radioactive gas. Looking at the decay chain in figure 6.6 the signals probably came from the alpha decay of Bi-212 and Po-212. Po-216 has a half-life of only 0.14 s and will therefore give contribute little while the other isotopes are not alpha emitters and will not be detected. The activity of the daughter isotopes reduces a lot after a couple of hours. The contribution from the background was small since the detector was operated at low gain.

The spectra from both the rock and the mantles are very broad. The source gave signals with all kinds of amplitudes but most signals with low amplitudes. This should not be surprising. Radon atoms are decaying randomly in the whole detector and the alpha particles are emitted in all directions. There will be signals from alpha particles which are amplified by four

GEM foils and some will probably not be amplified at all(and probably not seen). There will also be signals where only parts of the charge is collected on the pad being read out. The range of alpha particles are in the order of a few cm in gas. This means that in most cases only a small fraction of the ionization created by the alpha particles are collected on the pad being read out. All of this suggest that the spectrum should be broad and not give clear peaks corresponding to the energy of emitted alpha particles.

6.3 Lifetime study of the decay products of Rn-220

A study of the lifetime of the decay products of Rn-220 from the thorium mantles was performed with the GEM detector prototype. A goal was to determine the half-life of the daughter isotopes.

This was done by first let the detector gas with radon flow through the detector for about 20 hours to build up the amount of daughter isotopes of Rn-220. The mantles was then bypassed from the gas flow and a measurement of the energy spectrum was started about one minute after the mantles was bypassed. This measurement was performed for one hour. A new measurement was performed for one hour right after this. This was done ten consecutive times. These measurements made it possible to look at the number of counts at certain energy regions at different times after the radon supply was turned off. A background spectrum was also measured in order to determine the contribution from the background.

The large pad was used and the argon gas mix at flow rate of 3 litres per hour was used. The operating voltage was 3.1 kV. The signals was read out with the SAMPA chip and the maximum amplitude stored using LabView [13].

The energy spectrum measured the first hour after the mantles were bypassed is shown in figure 6.16. The region up to about 1000 ADC channels gets contribution from the noise discussed in previous section. The region above about 5000 has few counts especially several hours after the mantles were bypassed. The lifetime of the decay products was therefore studied in the region from 1200 to 5000 ADC channels.

Figure 6.17 shows the number of pulses registered at different times in the region from 1200 to 5000 ADC channels. The number of counts from the background is subtracted from number of pulses. The number of counts the tenth hour after the mantles were bypassed is just above half of the number of counts measured the first hour. This indicates that the half-life of the decay products is about ten hours. This fits well with the half-life of the longest lived isotope of the daughter isotopes of Rn-220 which have a half-life of 10.5 hours. The other daughter isotopes have much shorter half-life.

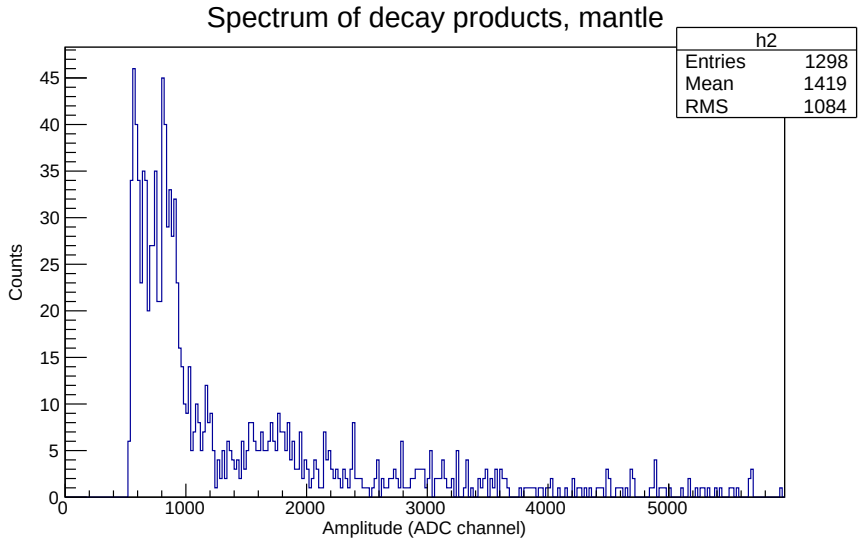

Figure 6.16: Energy spectrum of decay products measured to first hour after the mantles were bypassed from the gas flow.

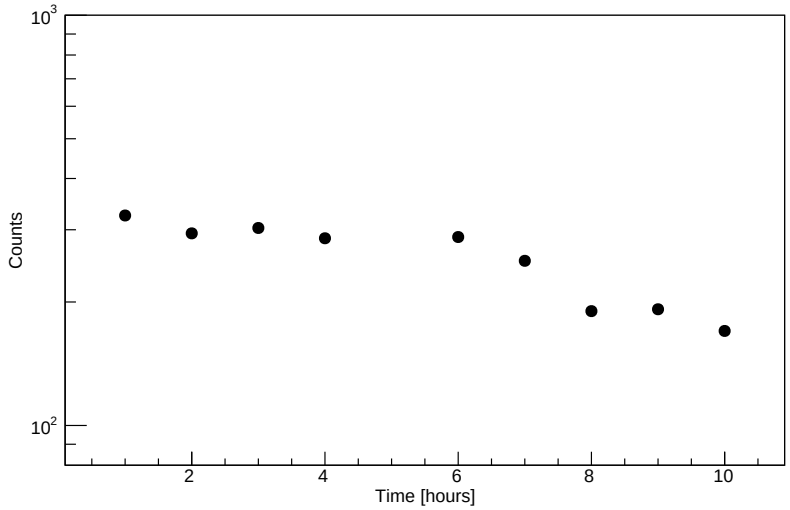

Figure 6.17: The number of counts from the daughter isotopes of Rn-220 registered every hour after the mantles were bypassed. The number of counts after ten hour is just above half of the counts registered the first hour.

6.4 Activity of the radioactive gaseous sources at different detector settings

An important quantity for spark studies is the rate of the radioactive sources used. The rate of radioactive decay of radon from both the rock and ten thorium mantles was measured using the GEM prototype detector, the SAMPA chip and the data acquisition system. The $Ar - CO_2(90 - 10)$ gas mix was flushed through the chamber containing the rock at a flow rate of both three and six litres per hour.

Measurements with both the large pad ($27 \times 27mm^2$) and a normal pad ($6 \times 15mm^2$) were done. Reading out an even larger area would be preferably since it would then be possible to more precisely tell what the activity in the whole detector was. This was not possible to do since the noise of the system became very high if many pads were connected due to the high capacitance of the large area being read out. It was therefore not possible to read out pulses with small amplitudes when reading out a large area of the detector. Even the measurements with the large pad gave a high noise. Figure 6.18a shows the noise of the large pad was up to about 500 ADC channels. The threshold of the DAQ system for measurements with the large pad was therefore set just above 500. Figure 6.18b shows that the noise for the $6 \times 15mm^2$ pad was only up to about channel 110 and the threshold was set just above this value. Keeping a lower threshold when measuring with a $6 \times 15mm^2$ pad compared to the large pad means that the system are able to measure signals with low amplitude better.

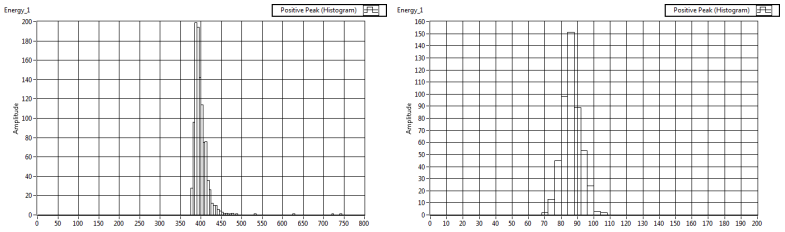

(a) Noise when measurements with the large pad was done.

(b) Noise when measurement with a $6 \times 15mm^2$ pad was done.

Figure 6.18: Noise from two different pads.

The detector gas with the radon gas was flushing through the detector for about one hour before the measurement was done in order to get rid of the accumulated radon in the container with the rock or the mantles and to build up activity from daughter isotopes. This will be similar to conditions if the rock or the mantles is going to be used as a source for other experiments.

The apparent activity from the source was expected to vary when varying the GEM operating voltage. Both the background and the source was measured at different operating voltages.

The number of pulses in a certain period of time were stored using the DAQ system and LabView. This was used to calculate the decay rate. Measurement with both the source and without the source was done in order to find the contribution from the background. The number of counts from the background were subtracted from the number of counts measured with the source to find the number of counts from the source. There might be some contribution of some irregular pickup noise. The approximated number of counts from the source was divided by how long the measurement was performed in order to find the measured rate. The result is shown in figure 6.19

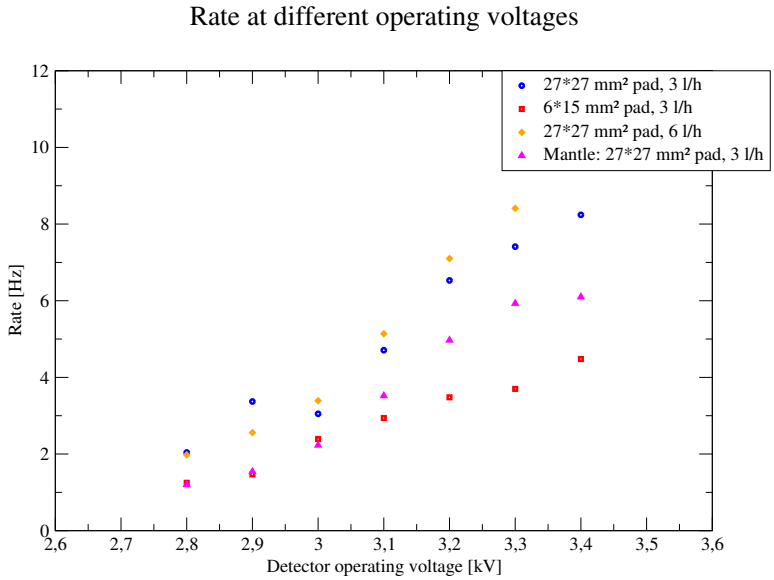

Figure 6.19: The count rate of the source measured with the large pad and one normal pad.

Firstly the results show that the activity from the Rn-220 from the rock was higher when reading out a large area ($27 \times 27mm^2$) compared to a smaller area ($6 \times 15mm^2$) even though the threshold was higher. Secondly, the results show that the higher gas flow rate will not give a much higher rate. It seems like the gas can not transport more radon gas at higher gas flow rate or that there is not more gas available from the rock to be transported. Lastly the results show that the Rn-220 from the rock gave higher rate than the ten mantles used. Using more mantles as a source would probably change this.

6.5 Spark testing

If discharges are happening and making a conducting bridge between some electrodes, it means that that the electrodes are shorted and the potential difference between them is reduced reduced for a while. Monitoring the voltage on the electrodes of the GEM detector will allow measurements of when discharges are happening. In most cases it is propagating discharges to the readout anode which are most interesting. The reason for this is propagating discharges conduct a lot of charge to the readout pad and the front end electronics. This may damage or destroy the electronics.

The procedure to measure discharges is to monitor the voltage on the electrodes. Figure 6.20 shows the voltage on one electrode when a discharge is happening. The voltage changes fast before it also recovers fast.

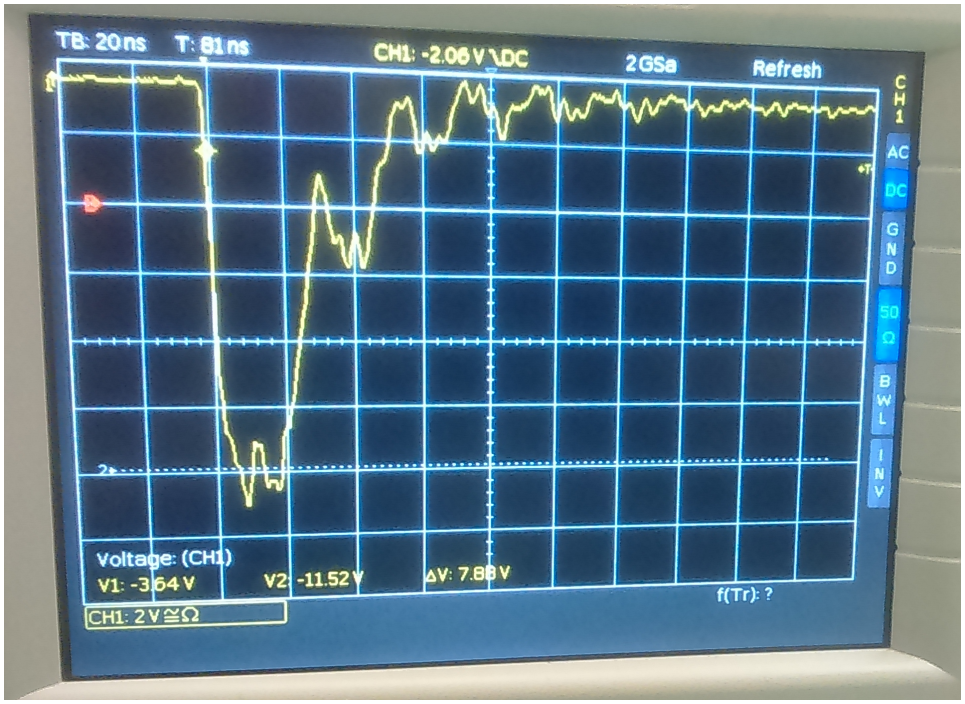

Figure 6.20: Oscilloscope picture of the voltage on one electrode when a discharge is occurring

Propagating discharges are measured by monitor the voltage on the bottom of the last GEM foil. If an propagating discharge to readout anode happens, a conducting bridge from the last GEM foil to the anode will be created. This means that the last GEM foil will be shorted to the ground. This is showed in figure 6.21. The top line shows that there is a signal from the detector or in other words, charges are reaching the readout pad. The bottom line shows the voltage on the last GEM foil. It changes from the

nominal level when a discharge is happening before it goes back to normal after the discharge.

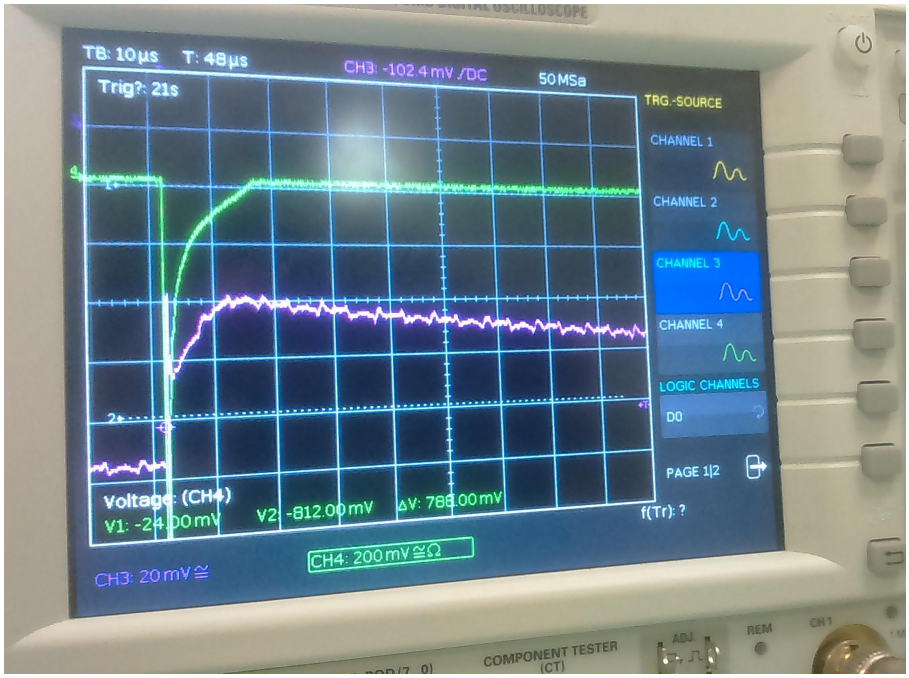

Figure 6.21: Oscilloscope picture of an propagating discharge. The top line shows the ordinary signal from the detector while to bottom line shows the voltage on the bottom part of the last GEM foil. The voltage in the GEM foil is going towards ground which means that the foil is shorted to ground.

6.5.1 Discharge testing with Am-241 source

Discharge testing with the GEM prototype detector was performed with an external Am-241 alpha source. The count rate was about 1 kHz. The detector gas used for this measurement was the $Ne - CO_2 - N_2$ (90-10-5) gas mixture.

Sparks were not observed at nominal voltage of 3.55 kV (gain of 2000). The voltage was increased to 3.9 kV and still no sparks were observed. At voltage of 3.93 kV and gain of about 10 000 sparks were observed approximately every second. Increasing the voltage to 4.0 kV increased the spark rate to a few sparks every second. At this setting sparks were observed even without any radioactive source. The sparks probably came from cosmic particles.

6.6 Protection circuit

It is important to have a protection circuit in front of the front end electronics in order to eliminate probability of damage the electronics. When spark testing was performed with an Am-241 alpha source the connected channel of the SAMPA chip was broken after the first spark. As a protection circuit there was diodes both before the SAMPA chip and the internal diodes of the chip. There was no resistor at the input of the SAMPA chip. Figure 6.22 shows oscilloscope picture of the first and the second spark that was observed.

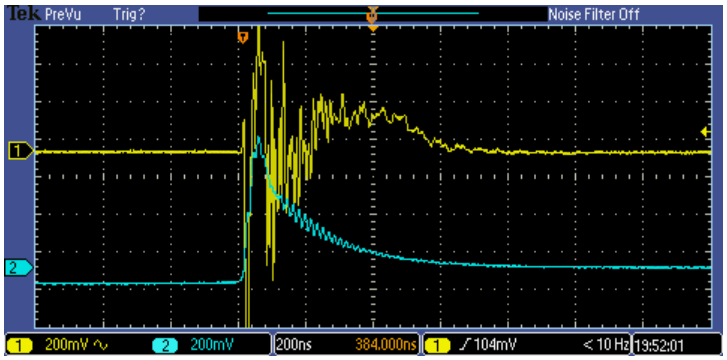

(a) A lot of charge is conducted to the front end electronics when the spark is happening.

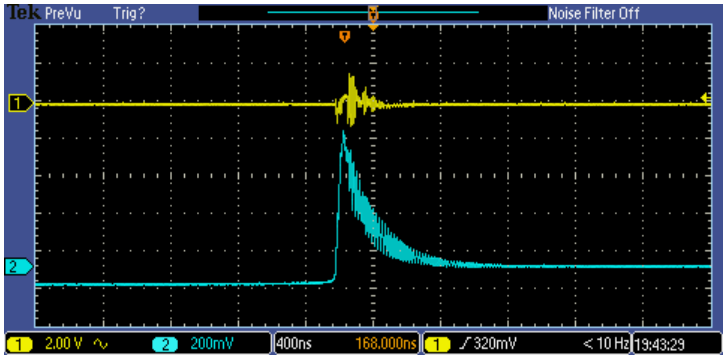

(b) The SAMPA chip gives not a proper output signal when the discharge is happening because the channel in use was already destoyed

Figure 6.22: Oscilloscope pictures of the first spark is shown in the top picture and the second spark in the bottom picture. The signal at the top (yellow) is the signal from the SAMPA chip and the signal at the bottom (blue) is the voltage of the last GEM.

The bottom line in both of the oscilloscope pictures in figure 6.22 show that discharges propagates to the anode. The voltage quickly goes towards ground and recovers fast when the discharge is over. The top line in figure

6.22a shows that a lot of charge is conducted to the input of the SAMPA chip. In figure 6.22b no signal is coming from the SAMPA chip when the discharge is happening. The reason for this was that the channel in use was broken after the first spark. This means that the protection circuit with only diodes in front of the SAMPA chip gives little protection when discharges occur. Therefore it is important to have a resistor at the input of SAMPA for protection. An example of an improved protection circuit is viewed in figure 3.5 in chapter 3. This will limit the charge transported to the chip and reduce the probability of discharges harming the chip. The drawback of having adding a resistor is that it might increase the noise.

6.7 Comparison of the signals from different radioactive sources

Screenshots of the pulses from the different sources was stored using an oscilloscope in order to compare the signals from the detector and the SAMPA readout chip. All of these measurements were done reading out a $4 \times 7.5mm^2$ pad in the $Ar - CO_2(90 - 10)$ gas mix. The measurements had to be done on a smaller pad since only the smaller pads had a thin polymer window which made measurements with an external alpha source possible. The gain varied since the detector could not be operated at the same settings for all radiations. Only the positive signals from the differential signals from the SAMPA chip are shown.

One of the parameters to look at was the peaking time of the signal.

The sources were the same as earlier. The X-ray source was Fe-55, the beta source was Sr-90/Y-90 and the alpha source was both the Am-241 source and Rn-220 flushed from the rock.

6.7.1 X-ray source

The detector could as earlier run at normal gain of about 2000. Three screenshots is shown in figure 6.23. The pulse shape looks fine but the peaking time was not stable. Most pulses seemed to have peaking time of 160 ns but but both longer and shorter peaking time was observed frequently. The signal in figure 6.23b has a peaking time of 210 ns while the signal in figure 6.23c has a peaking time of 150 ns. This means that the SAMPA chip did not perform optimal during this test.

There was little pile-ups of the pulses even though the high rate of 3.7 MBq of the Fe-55 source. The amplitude of the X-ray pulses was mostly in range of some hundred mV.

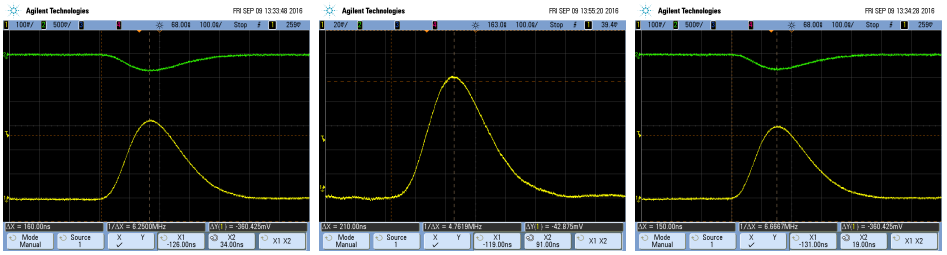

(a) Peaking time: 160 ns (b) Peaking time: 210 ns (c) Peaking time: 150 ns

Figure 6.23: Screenshots of X-ray signals. The left pictures shows a pulse with peaking time of 160 ns. The two others shows signals where the peaking time is deviating from this. The signal in the middle and to the right have peaking time of 210 ns and 150 ns, respectively.

6.7.2 Beta source

The GEM detector prototype was operated at gain of about 2000. Screenshots of beta pulses are shown in figure 6.24. The peaking time seemed to be quite stable at 160 ns. The amplitude was mostly in the range of some tens of mV. There were very little pile ups for the beta pulses.

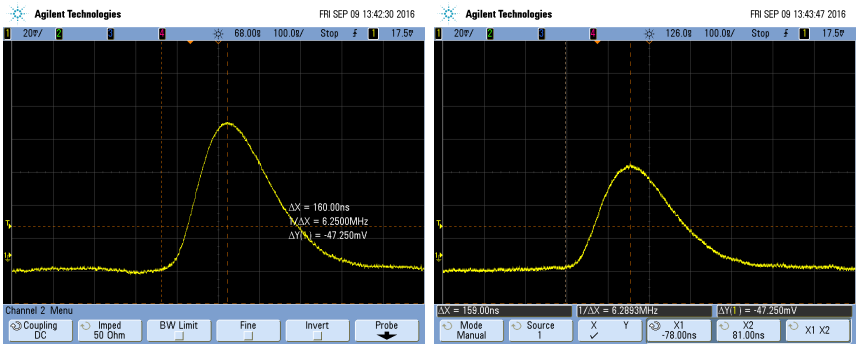

Figure 6.24: Screenshots of beta signals. The peaking time was observed to be 160 ns.

6.7.3 Alpha sources

Since the alpha particles are heavily ionizing the detector was run at a low gain. The alpha signal came from different sources.

Pictures of the signals from the Am-241 source are shown in figure 6.25. It is important to note that signal does not fall to the baseline as fast as the signal from the other sources. Together with the high activity of 34.7 kBq and the long interaction time the pulses become highly piled up. One signal

therefore contains the ionization product from several alpha particles

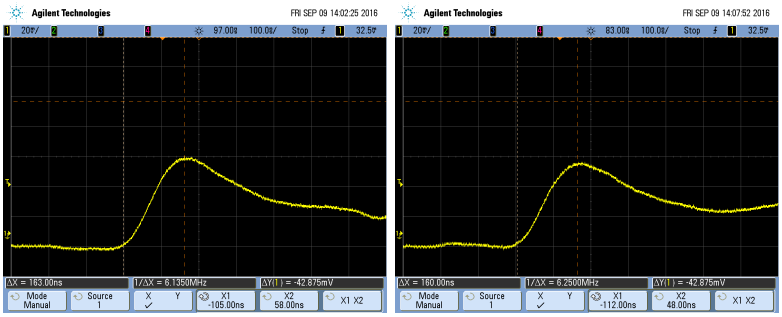

Figure 6.25: Screenshots of the signals of the alpha particles from a Am-241 source. The signals are piled up. The peaking time was stable around 160 ns.

Figure 6.26 shows the signals from the alpha particles from the radon gas. This signal is not piled up due to the low rate of this source.

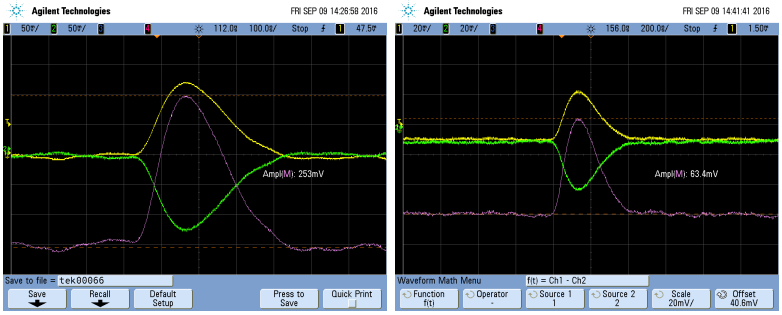

Figure 6.26: Screenshots of the signals of the alpha particles from the radon gas coming out of the rock. The peaking time was about 160 ns.

6.8 Ageing of the detector

Ageing of a detector means that the detector gets permanent damage when irradiated resulting in a deterioration of performance.

The relative resolution of the Fe-55 photon peak was found again after performing experiments with the beta source and the alpha sources. The resolution was found the same way as described in section 4.2. The fitted energy spectra both before and after all the testing are viewed in figure 6.27. Both of the energy spectra are measured in the $Ar - CO_2(90 - 10)$ gas mix reading out the large pad. The operating voltage was 3.8 kV giving a gain of about 2000.

The relative resolution measured in the beginning of this project was about 15 % at the given detector operating settings. At the end the relative resolution was measured to be about 20 %. This shows that the resolution after a lot of testing with the GEM detector prototype was clearly lower. This suggest that the detector has been harmed by the use. It is most likely that it is the alpha particles that have been harmful. The alpha particles are heavily ionizing and lose a lot more energy per unit length compared to the beta particles. Since there large pad has not been tested with the Am-241 source because there is no thin polymer window above the large pad the damage has to come from the radon sources.

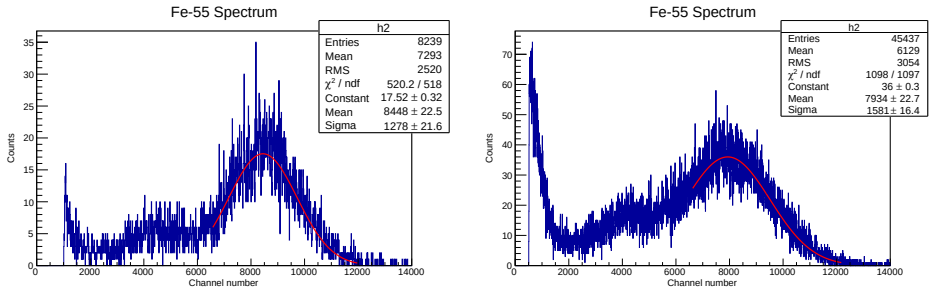

Figure 6.27: The relative resolution of the detector measured with a Fe-55 source. The left figure shows the spectrum measured early in this project. The resolution was then measured to about 15 %. The right spectrum was measured at the end of this project. The resolution was then about 20 % .

Chapter 7

Summary and Conclusions

The LHC upgrade before Run 3 in 2018 will increase the interaction rate and energies of the collisions. To meet the new requirements set by the increased interaction rate and increased collision energy after the upgrade the ALICE TPC needs to be upgraded. The TPC currently uses multiwire proportional chambers for readout but this will be replaced by GEM based readout system. Along with the new GEM detectors a new front end electronic chip called SAMPA will be used.

The first objective of this thesis was to test a GEM detector prototype with different kinds of radioactive sources and compare the response. The second objective was to make a setup for discharge studies with the GEM detector prototype and to characterize two radioactive radon sources used to make discharges.

The GEM detector prototype was first tested with a Fe-55 X-ray source for gain calibration and measurement of the relative energy resolution. The gain was determined at different voltages, detector gases and gas flow rates. The relative energy resolution was measured at different detector settings. The resolution of 5.9 keV photons at nominal gain of 2000 was found to be 12 % which meets the requirement for the ALICE TPC. This is however much lower resolution compared to a GEM detector with standard configuration. The GEM detector prototype has the same foil arrangement (S-LP-LP-S) and voltage as the detectors that will be used in the ALICE TPC. The detector is designed to give a very low ion backflow to minimize the disturbance of the electric field of the TPC. This configuration is making the energy resolution lower than for standard configurations.

The detector was also tested using minimum ionizing particles from a Sr-90 beta source. A plastic scintillator was used as an external trigger as well as to discriminate the low-energy electrons emitted by the source. Because of the noise of the detector system and the low energy loss of the minimum ionizing beta particles the gain needed to be above the nominal gain of 2000 in order to get a good measurement of the Landau distributed energy loss.

Discharges are a limiting factor for GEM detectors. If there is too much charge in an avalanche a breakdown of the gas may happen. Large amount of charge may be conducted to one of the electrodes. This may harm the detector or the front end electronics if the discharge is propagating to the read out anode. The detector was therefore tested with alpha sources since alpha particles are heavily ionizing and most capable to induce discharges. The detector had thin polymer windows which allowed the use of external Am-241 alpha sources. This source gave a high rate of about 1 kHz which lead to pile-ups of pulses. The pile-ups were reduced by adding collimators. The energy loss distribution seemed to be approximately Gaussian.

The detector was also tested with an internal radioactive gas as a source. The gas was flushing through a container with either a rock containing thorium and thorium enriched mantles before entering the detector. Rn-220, a daughter isotope of Th-232, was then transported with the gas into the gaseous volume and emitted alpha particles and thus creating signals in the detector. The rate of signals from both of these sources was measured. The rate varied with voltage and size of the area read out. The largest area read out was the large pad ($27 \times 27 mm^2$). A large area would give better results but this was not possible due to high noise and oscillations of SAMPA chip. The rate measured with the large pad was up to about 8 Hz for the rock and up to about 6 Hz for ten mantles. This means that measuring small discharge probabilities would be difficult with this setup.

Spark testing with the Am-241 source was done. No sparks were observed at gain of 2000. Sparks were first visible at gain roughly five times higher. The first spark observed transported so much charge to the SAMPA chip that the channel in use became broken. There were diodes for protection but no resistor in front of the read out chip. This indicates that a better protection circuit possible with a resistor, is needed to protect the SAMPA chip better.

The relative energy resolution of the GEM detector prototype was measured again after a lot of testing with the detector. The resolution decreased from 15 % to 20 % for a typical detector operating setting. This suggests that the detector was harmed by the alpha particles from the radon sources.

Bibliography

[1] L. Evans and P. Bryant, *LHC Machine*. 2008.

[2] The ALICE collaboration, *The ALICE experiment at CERN LHC*, Journal of Instrumentation. 2008.

[3] The ALICE collaboration, *Technical design report for the upgrade of the ALICE time projetion chamber*. 2014 .

[4] W. R. Leo. *Techniques for Nuclear and Particle Physics Experiments*. 2nd Rev. Springer, 1994.

[5] C. Patrignani et al. (Particle Data Group). Passage of particles through matter. *Chinese Physics C*, (p. 441-455). 2016.

[6] C. Grupen and B. Shwartz, *Particle Detectors*, Second Edition, Cambridge University Press. 2008.

[7] F. Sauli, *The Gas Electron Multiplier(GEM): Operating principles and applications* Nuclear Instruments and Methods in Physics Research A. 2015.

[8] S. Bachmann, A. Bressan, M. Capeáns, M. Deutel, S. Kappler, B. Ketzer, A. Polouektov, L. Ropelewski, F. Sauli, E. Schulte, L. Shekhtman, A. Sokolov. *Discharges studies and prevention in the gas electron multiplier (GEM)*. Nuclear Instruments and Methods in Physics Research A. 2000.

[9] A. Bressan, M. Hoch, P. Pagano, L. Ropelewsko, F. Sauli, S. Biagi, A. Buzulutskov, M. Gruwe, G. De Lentdecker, D. Moermann, A. Sharma. *High rate behavior and discharge limits in micro-pattern detectors*. uclear Instruments and Methods in Physics Research A. 1999.

[10] E. Noschis et al., *Protection circuit for the T2 readout electronics of the TOTEM experiment*, Nuclear Instruments and Methods in Physics Research A 572, (378-381). 2007

[11] Fig: Thorium decay chain. `https://en.wikipedia.org/wiki/Decay_chain#/media/File:Decay_Chain_Thorium.svg`

[12] Kristian P. Engeseth, *ALICE TPC Upgrade Activities for LHC Run 3 and Beyond: "SAMPA ASIC Tests with GEM Detector Prototype"*. Master Thesis. University of Bergen. 2015.

[13] LabVIEW. http://norway.ni.com/labview.